CHAPTER II

HISTORY

CLASSIFICATION OF COUMARINS

Coumarin is applied to a large group of naturally occuring compounds possessing a 2H-1-benzopyran-2-one nucleus. In 1820, coumarin was first isolated from seed of *Coumarona ordorata* Aubl. by Vogel. Unitie now, about 300 coumarins have been isolated from many source of plants, especially from families Gramineae, Guttiferae, Leguminosae, Orchidaceae, Rutaceae and Umbelliferae (7). They have also been reported from microorganisms (8) and animals (9).
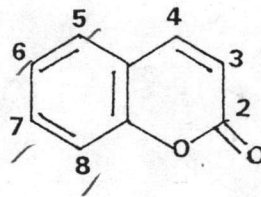
Coumarin nucleus

(2H-1-benzopyran-2-one nucleus)

No completely satisfactory classification of the coumarins is possible at present. Steck and Mazureck (10) have divided coumarins into two types. One is "normal" type, which has an oxygen function at C-7 and hydrogen at C-3 and C-4 unsubstituted pyrone ring). The other is

"abnormal" type, which either lacks of the C-7 oxygen or possesses pyrone ring substituents. Seshadri and Vishwapaul (8) have classified coumarins into five groups as following.

1. Simple coumarins

This type of coumarins is possessed a 2H-1-benzopyran-2-one nucleus (coumarin nucleus) and there are side chains substituted on benzene ring of the benzopyran nucleus. 7-oxygenated coumarins are the most common in this type. There are widely distributed of simple coumarins in Rutaceae and Umbelliferae.
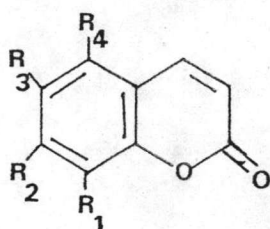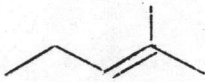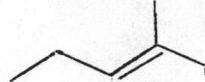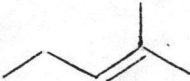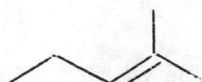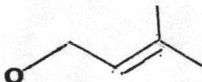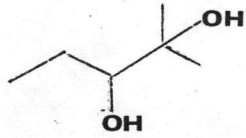
Table 1   The example of some simple coumarins

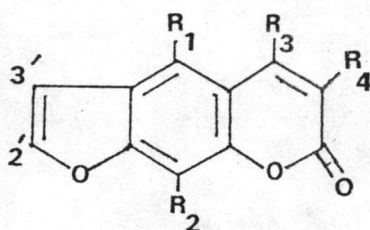| Name	R_1	R_2	R_3	R_4
Umbelliferone	H	OH	H	H
Aesculetin	H	OH	OH	H
Scopoletin	H	OH	OMe	H
Suberosin	H	CH₃	[alkenyl chain structure]	H
Peucedanol	H	OH	[alkenyl chain structure]	H
Coumurrayin	[alkenyl chain structure]	OMe	H	OMe
Brayleyanin	[alkenyl chain structure]	[O‑prenyl structure]	OMe	H
Ulopterol	H	OMe	H	[hydroxyl chain structure]

2. Furanocoumarins

This type of coumarins has furan ring which is fused with the coumarin nucleus at the various positions on benzene ring to form linear or angular structure. Furanocoumarins can be classified, considering the fusion of furan ring, into six subtypes.
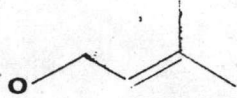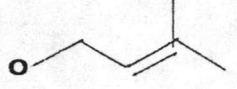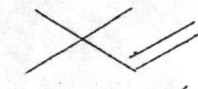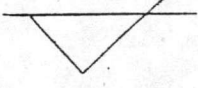
5

2.1 Psoralene type (linear)

This type of coumarins has furan ring fused with the benzene ring at C-6 and C-7 positions as a linear structure. The double bond occured at C-2′, C-3′ and there are side chains substituted at the various positions on coumarin nucleus.

Psoralene nucleus

Table 2   The example of some psoralene type coumarins

Name	R_1	R_2	R_3	R_4
Psoralen	H	H	H	H
Xanthotoxol	H	OH	H	H
Bergaptol	OH	H	H	H
Imperatorin	H	O—	H	H
Phellopterin	OMe	O—	H	H
Chalepensin	H	H	H	
Clausindine	H	H	H	
Halkendin	H	H	OMe	OMe
Halfordin	OMe	H	OMe	OMe
Isohalfordin	H	OMe	OMe	OMe

2.2 Angelicin type (Angular)

This type of coumarins has furan ring fused with the benzene ring at C-7 and C-8 and there are side chains substituted at the coumarin nucleus. At C-2′ and C-3′ has one double bond.
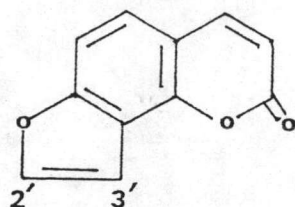
Angelicin type
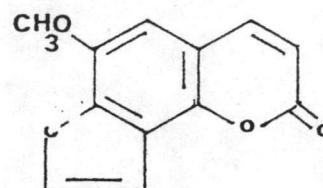
Sphondin
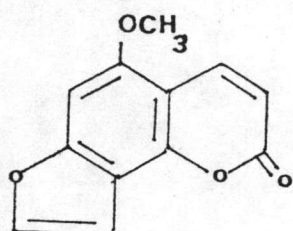
Isobegapten
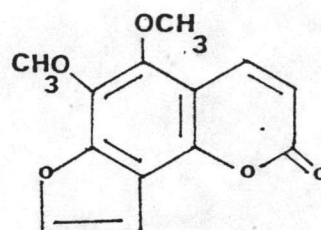
Pimpinellin

2.3 Dihydrofuranocoumarin [4,3] type

This type has furan ring fused with benzene ring at C-3 and C-4 positions. There is no double bond at C-2´ and C-3´but there are substituents in the side chains.
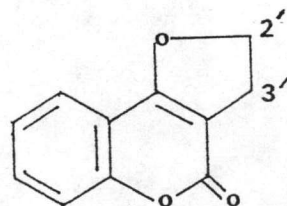
Dihydrofuranocoumarin [4,3] nucleus
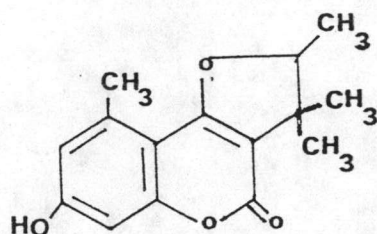
Glaupalol

2.4 Dihydrofuranocoumarin [5,6] type

This type has furan ring fused with the benzene
ring at C-5 and C-6 positions. There is no double C-2´and
C-3´.

Dihydrofurnocoumarin [5,6] nucleus
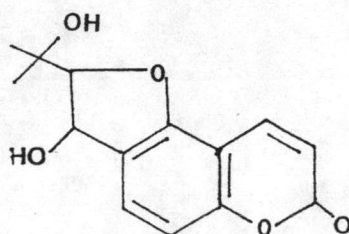
Xanthoarnol

2.5 Dihydrofuranocoumarin [7,6] type

This type has furan ring fused with the benzene ring at C-6 and C-7 positions as same as in psoralene type, but there is no double bond at C-2′ and C-3′ positions.
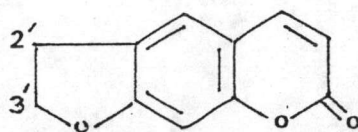
Dihydrofuranocoumarin [7,6] nucleus
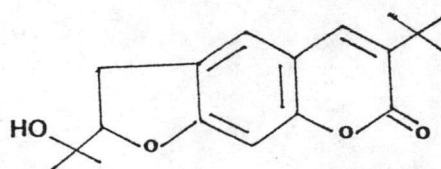
Chalepin (heliettin)
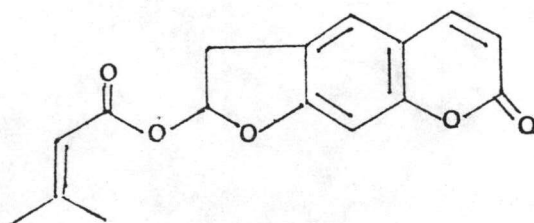
Prantschimgin
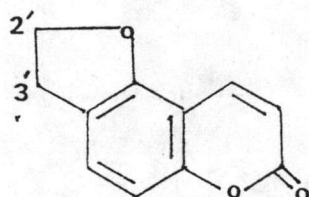
2.6 Dihydrofuranocoumarin [7,8] type

This type has furan ring fused with the benzene ring at C-7 and C-8 positions as same as in angelicin type, but there is no double bond at C-2′ and C-3′ positions.
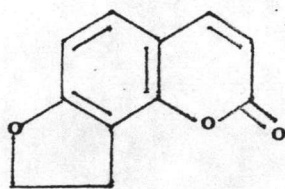
Dihydrofuranocoumarin [7,8] nucleus
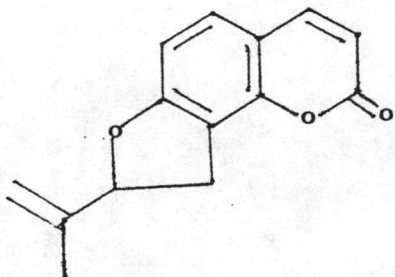
Angenomalin
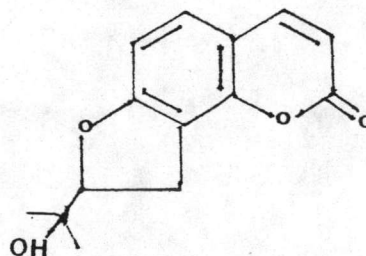
Columbianetin

3. Pyranocoumarins

This type of coumarins has pyran ring which is fused with the coumarin nucleus at the various positions on benzene ring to form linear or angular pyranocoumarin. These coumarins may be called chromano-coumarins.

Pyranocoumarins have been classified, considering the fusion of pyran ring, into five subtypes (10).
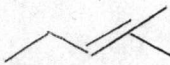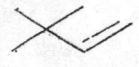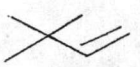
3.1 Xanthyletin type (linear)

This type has pyran ring fused with the benzene ring at C-6 and C-7 position as a linear type. The hydrogen at C-2' is substituted with two methyl groups and there is one double bond at C-3' and C-4'.
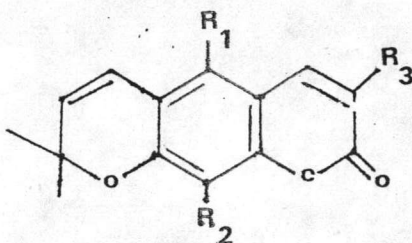
Xanthyletin (linear) nucleus

Table 3   Xanthyletin linear pyranocoumarins type

Name	R_1	R_2	R_3
Xanthyletin	H	H	H
Xanthoxyletin	OMe	H	H
Luvangetin	H	OMe	H
Trachyphyllin	OH		H
Poncitrin	OMe		H
Clausarin	OH		
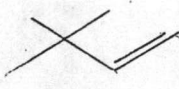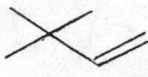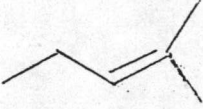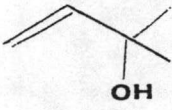
3.2 Xanthyletin type (Angular)

This type of pyranocoumarin is as same as xanthyletin linear type but the pyran ring fused position is C-5 and C-6 in stead of C-6 and C-7.
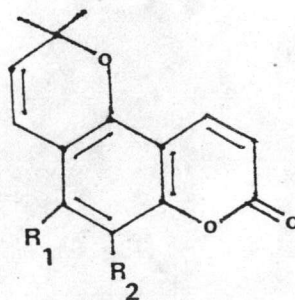
Xanthyletin (angular) nucleus

Table 4   Xanthyletin angular pyranocoumarins type

| Name | R₁ | R₂ |

Name R_1 R_2

Name	R_1	R_2
Alloxanthoxyletin	OMe	H
Dentatin	OMe	
Nordentatin	OH	
Dipetaline	OMe	
Avicennin	OMe	
Avicennol	OMe	

3.3 Seselin type

This type of pyranocoumarin has pyran ring fused with the benzene ring at C-7 and C-8 positions. The C-2′ is substituted with two methyl groups and there is one double bond at C-3′and C-4′(8).
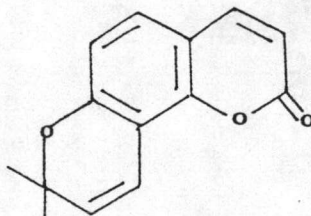
Seselin nucleus
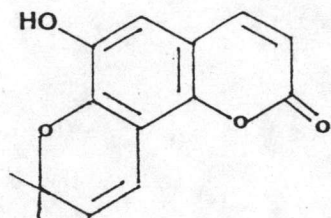
Norbraylin
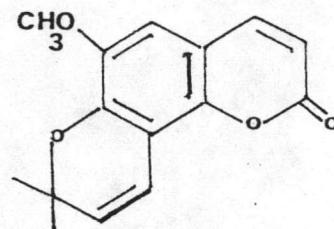
Braylin

3.4 Dihydroxanthyletin type

The structure of this type is as same as xanthyletin type (linear) but there is no double bond at C-3' and C-4'.
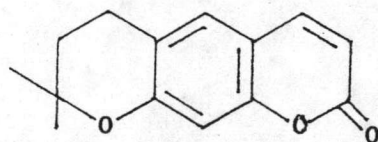
Dihydroxanthyletin nucleus
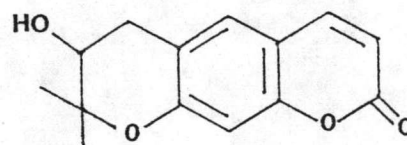
Decursinol
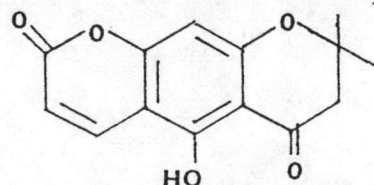
Clausenin
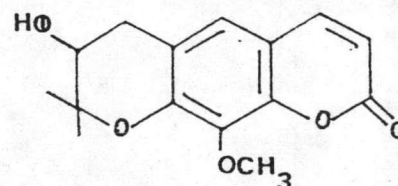
Arnottianin

3.5 Dihydroseselin type

The structure of this type is as same as seselin type but between C-3´ and C-4´ has no double bond.
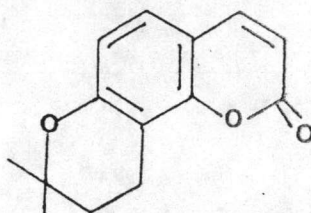
Dihydroseselin nucleus
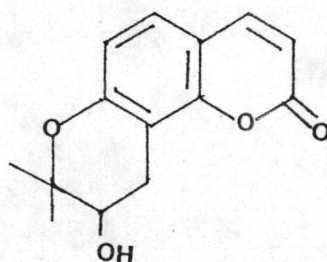
Lomatin

4. Phenyl coumarins

This type of coumarins has phenyl ring substituted at C-3 or C-4 of coumarin nucleus. Phenylcoumarins can be classified into seven subtypes.

4.1 3-Phenylcoumarin type

There is phenyl ring substituted at C-3 of the simple coumarin nucleus in the structure of this type.
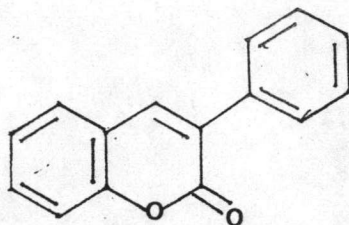
3-Phenylcoumarin nucleus
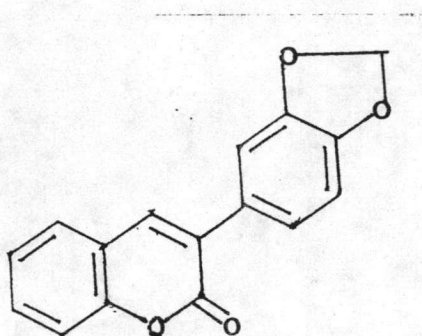
Derrussnin

4.2 4-Phenylcoumarin type

This type consists of phenyl ring substituted at
C-4 of the simple coumarin nucleus.
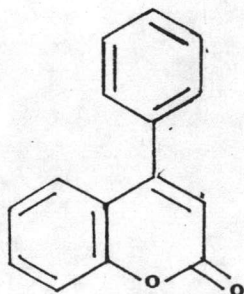
4-Phenylcoumarin nucleus
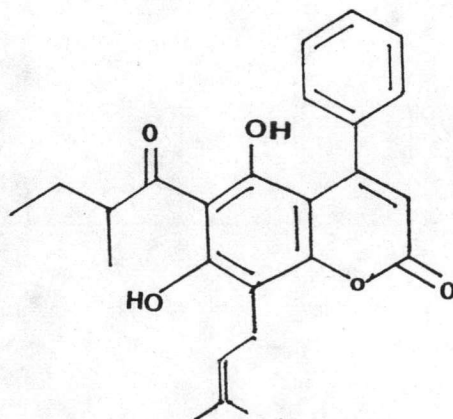
Mammea A/AB

4.3 4-Phenyldihydroangelicin type.

This type has phenyl ring substituted at C-4 of the dihydrofurano coumarin [7,8] nucleus.
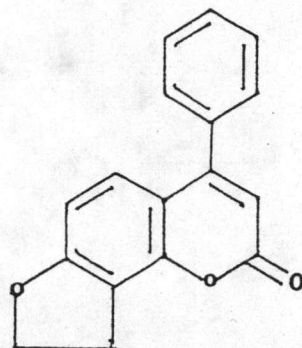
4-phenyldihydroangelicin nucleus

4.4 3-Phenyl xanthyletin type

There is phenyl ring substituted at C-3 of the xanthyletin linear nucleus.
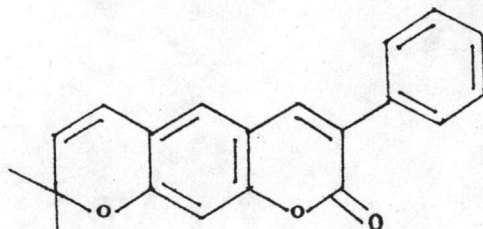
3-Phenylxanthyletin nucleus
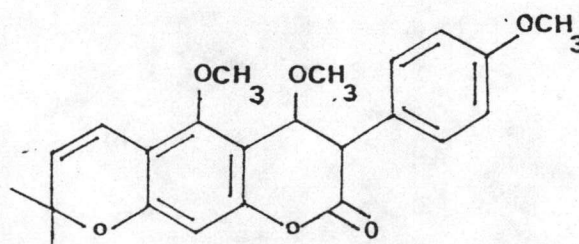
Robustic acid

4.5 3-Phenylseselin type

This type has phenyl ring substituted at C-3 of the seselin nucleus.
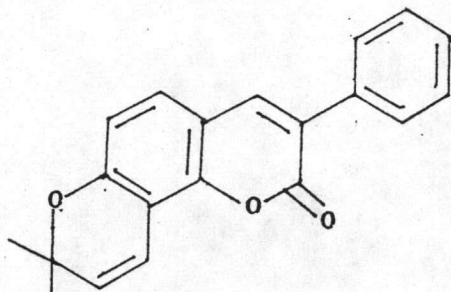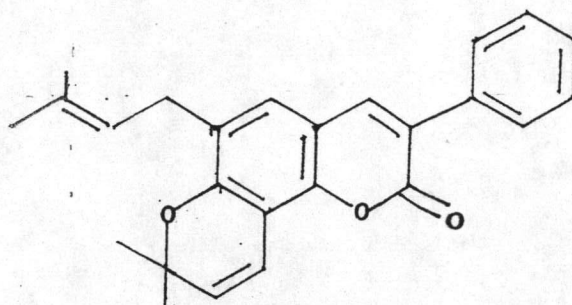
3-Phenylseselin nucleus   Scandanin

4.6 4-Phenylseselin type

This type consists of phenyl ring substituted at C-4 of the seselin nucleus.
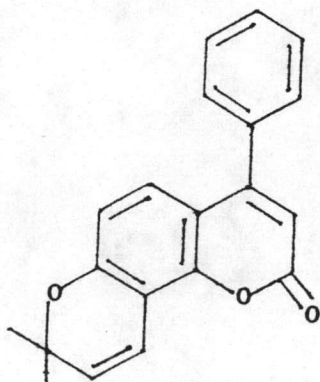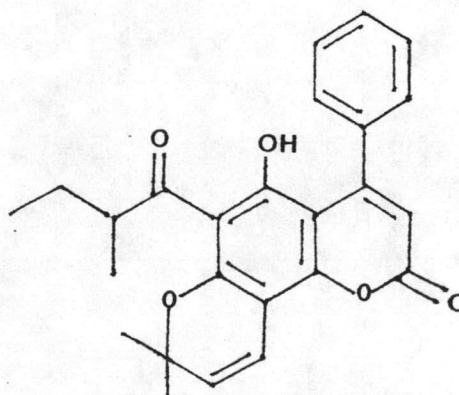
4-Phenylseselin nucleus   Mammeigin

4.7 Tripyran derivative type

There is two pyran rings and one phenyl ring in the structure of coumarin nucleus.
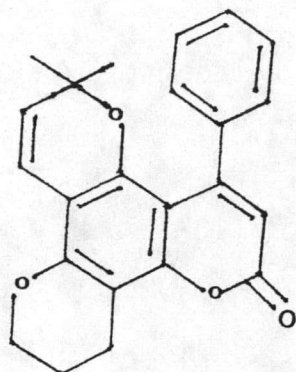
Tripyran nucleus
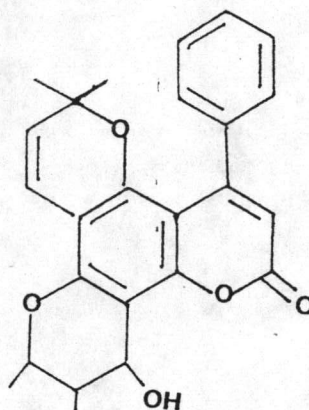
Inophyllum A

5. Bicoumarins

This type of coumarins consists of two coumarin nuclei bonded with or without methylene group (11).
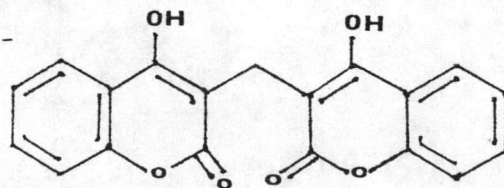
Dicoumarol
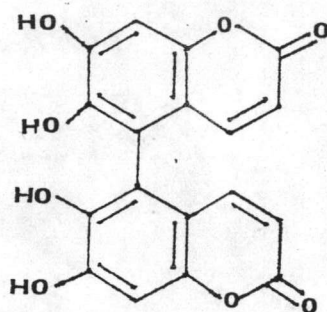
Euphorbetin

BIOSYTHESIS OF COUMARINS

The coumarins are typical metabolites of higher plants. The common precursors of the benzopyrone nucleus are phenylalanine and trans-cinnamic acid. Hydroxylation of the ortho-position of the cinnamic acid takes place first and then the 0-coumaric acid is subsequently glucosycolated. It is also rearranged in a spontaneous light-dependent reaction to the corresponding coumaric acid glucoside. By enzymetic elimination of glucose, free coumarinic acid is formed then cyclizes spontaneously to coumarin (Figure 1) and para-hydroxylation of trans-cinnamic acid is a necessary prerequisite for synthesis of the 7-hydroxycoumarins. Through 0-hydroxylation and lactonization as before (12,13). The ortho- and para-hydroxylation of trans-cinnamic acid are mediated by different enzymes.

The major feature in the diversification of simple coumarins in both Rutaceae and Umbelliferae is the widespread incorporation of prenyl unit. Prenylation has been demonstrated to occur at the umbelliferone stage which premits the electrophilic attack of carbonium ion at either C-6 or C-8 to yield C-prenyl coumarins or on the phenoxide to give O-prenyl compounds (Figure 1) (12,13).
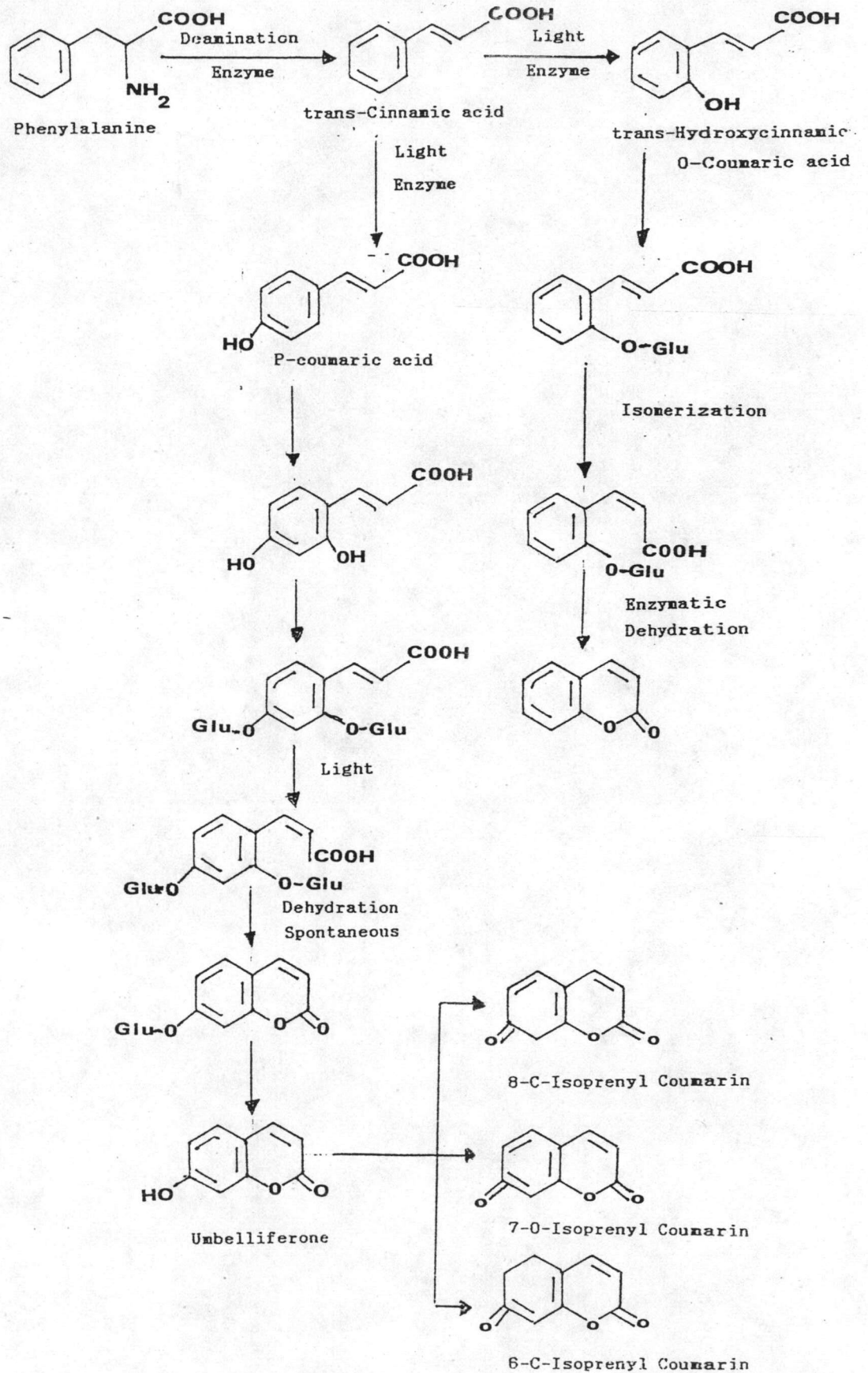
Figure 1   Pathway from phenyalanine to coumarins

Perhaps the role of the prenylating enzyme is to localize the charge on anion and to direct the attack of the prenyl unit (12). In *Ruta graveolens* L., the addition of dimethylallyl unit at C-6 appears to be specifically controlled by dimethylallyl phosphate tranferase (prenylase), which has a requirement of Mn^{2+} to form demethylsuberosin (DMS) (Figure 2).

Umbelliferone   Demethylsuberosin (DMS)
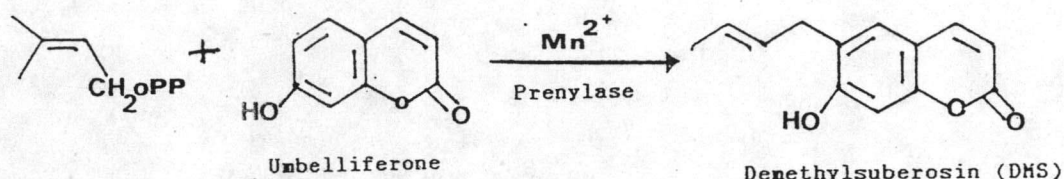
Figure 2   Formation of demethylsuberosin by prynylase

In more complex compounds, from tracer experiments have demonstrated that DMS is a precursor of linear furanocoumarins (marmesin) and osthenol is a precursor of angular furanocoumarins (angelcin) (Figure 3) (14). The mechanism is suggested that the carbocation at C-4´of marmesin is generated, following by 1,3-elimination, to yield acetone and psoralen (Figure 4) (13).
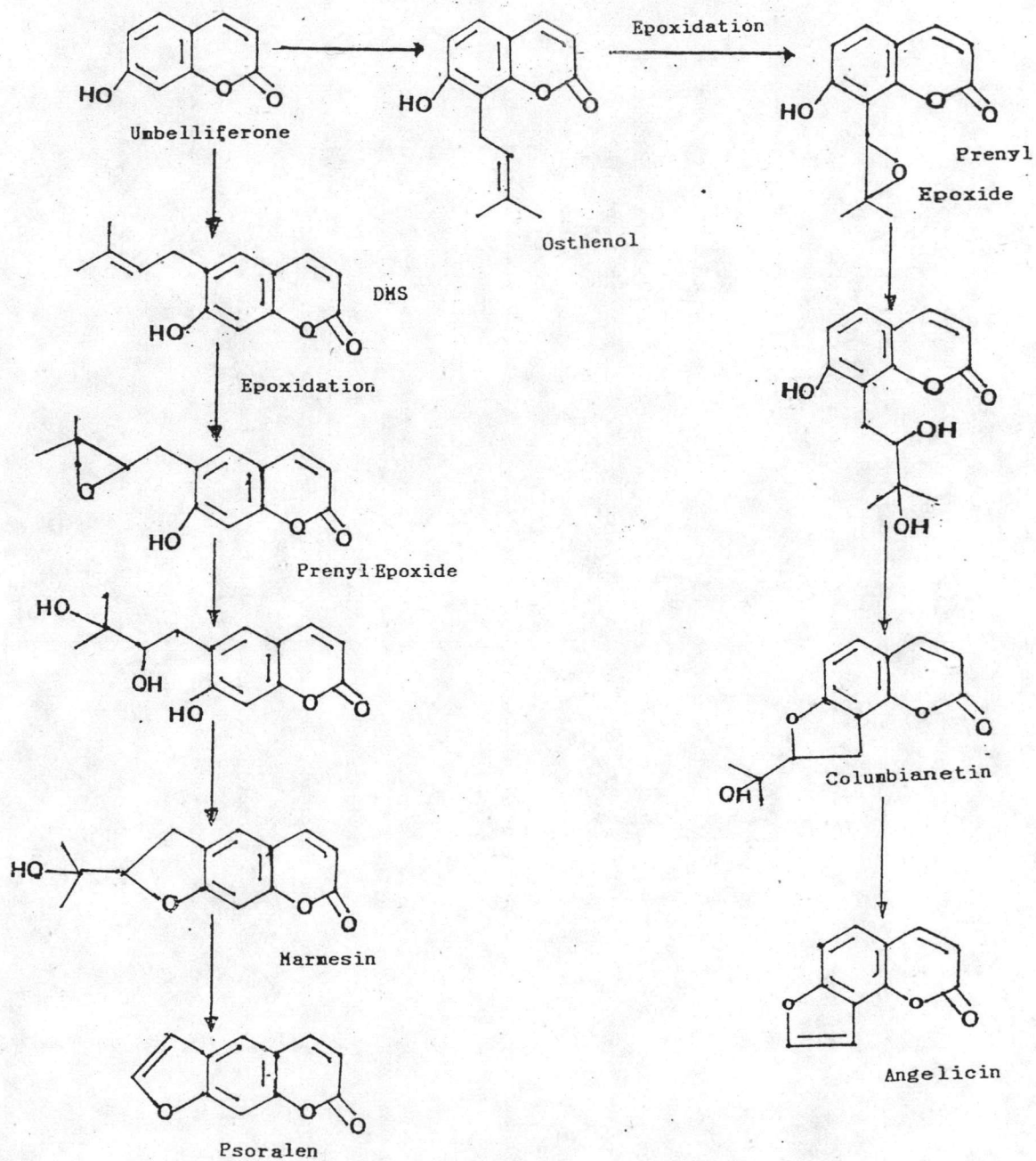
Figure 3   Hypothesis of linear and angular
furanocoumarins biosynthesis (14)
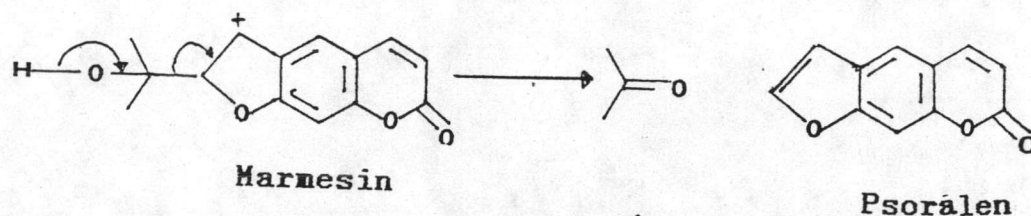
Marmesin

Psorálen

Figure 4   Mechanism proposed by Birch et.   al.
            for   conversion   of   marmesin   to
            psoralen

Although   no   details   investigation   into   the
information of pyranocoumarins has yet been reported.
The   observation   that DMS is heavily   incorporated   into
3´,4´-dihydroxanthylethin suggests a pathway analogous   to
that   for   furanocoumarins is in operation.   It has been
note that the configuration of the C-prenyl epoxide
intermediate   is   retained during the   formation   of
pyranocoumarins (Figure 5).   The xanthyletin   angular
pyranocoumarins are probably the products of cyclization
of a C-6 prenyl unit and free C-5 hydroxy substituents
(12).

Prenyl epoxide

Dihydrofuranocoumarin

Furanocoumarin

Dihydropyranocoumarin
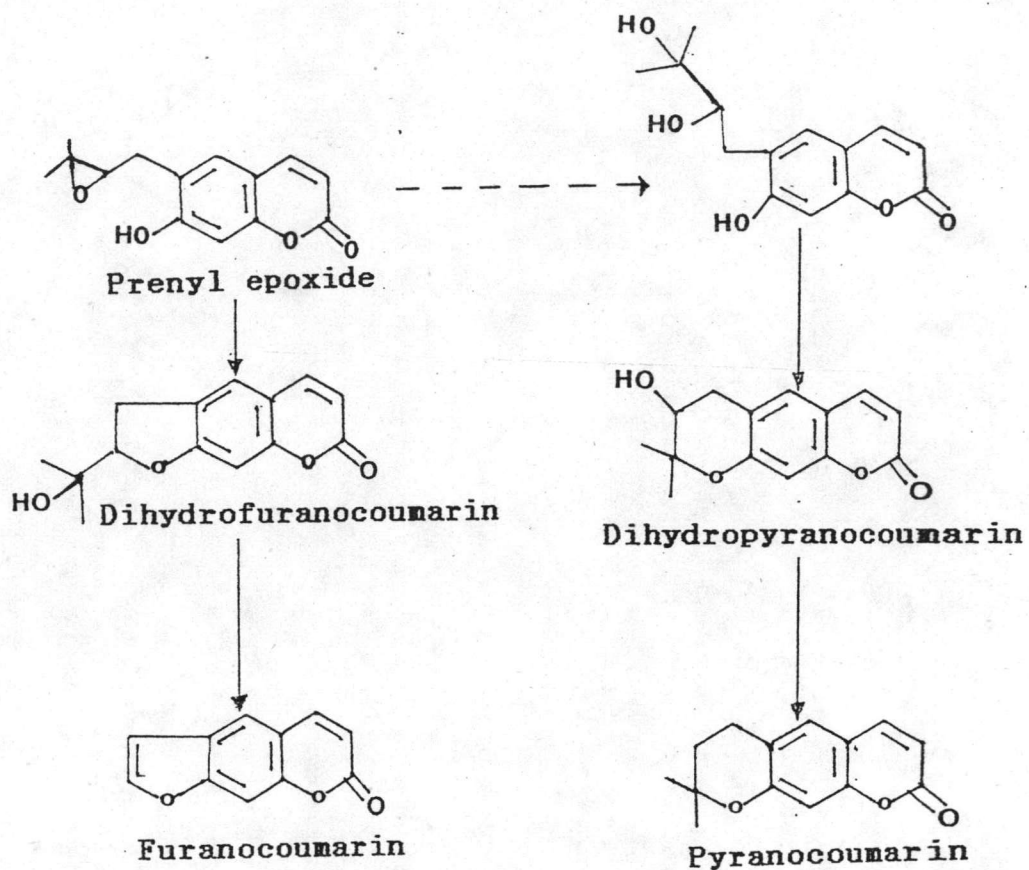
Pyranocoumarin

Figure 5   Formation of linear furanocoumarins and pyranocoumarins from 6-C-isoprenyl coumarin precursor (12)

PHYSIOLOGICAL ACTIVITY OF COUMARINS

From the studies of structure-activity relationship, it has found that several physiological properties of coumarins have related with their structures. For example, 3-phenyl coumarins, coumestrol, exhibit estrogenic activity. The highly substituted coumarin, novobiocin, is commercial antibiotic and some related 3-amino-4-hydroxy coumarins possess considerable antibacterial activity (15). Coumarins hydroxylated at C-4, such as dicoumarol, function as anticoagucants. The coumarins, micromelin and scopoletin, have isolated from Micromelum integeuimum and demonstrated to have antitumor activity (4) and microminutin, 7-methoxycoumarin, is a novel cytotoxic coumarin (3).

EXPERIMENTAL TECHNIQUES IN ^{13}C NMR

Assignment the chemical shift of carbon in ^{13}C NMR can be used several techniques in combinations to elucidate structure of organic compound. Some techniques are as following.

1. Proton-decoupling techniques

The initial ^{13}C experiments always record under proton noise decoupling. This is the most effecient recording mode, providing the chemical shift, ideally, the carbon number of the molecule. Some techniques, simple-double resonance methods, leading to spectra in which carbon-proton spin-spin couplings are partially or fully retained are as following

1.1 Proton noise decoupling (16)

Proton noise decoupling technique increases signal to noise and simplifies the complex ^{13}C NMR spectra because the irradiation frequency is to simultaneously remove all carbon-proton scalar couplings. The proton noise decoupled ^{13}C NMR spectrum of brucine is displayed in Figure 6.
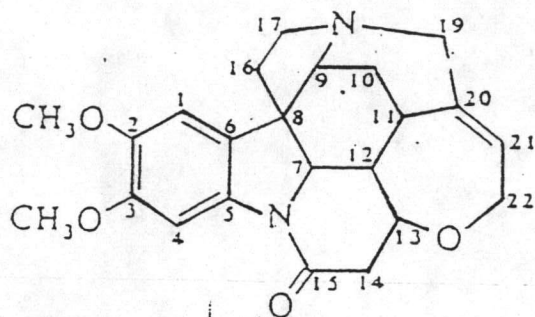
No.	Int.	ppm	No.	Int.	ppm
1	128	168.63	13	148	59.81
2	91	149.13	14	185	56.44
3	59	146.13	15	205	56.04
4	125	140.28	16	110	52.57
5	84	135.97	17	163	51.82
6	134	127.13	18	106	50.04
7	111	123.46	19	138	48.15
8	125	105.88	20	119	42.34
9	118	101.08	21	134	42.20
10	134	77.62	22	128	31.50
11	110	64.43	23	94	28.72
12	154	60.22	24	82	0.00
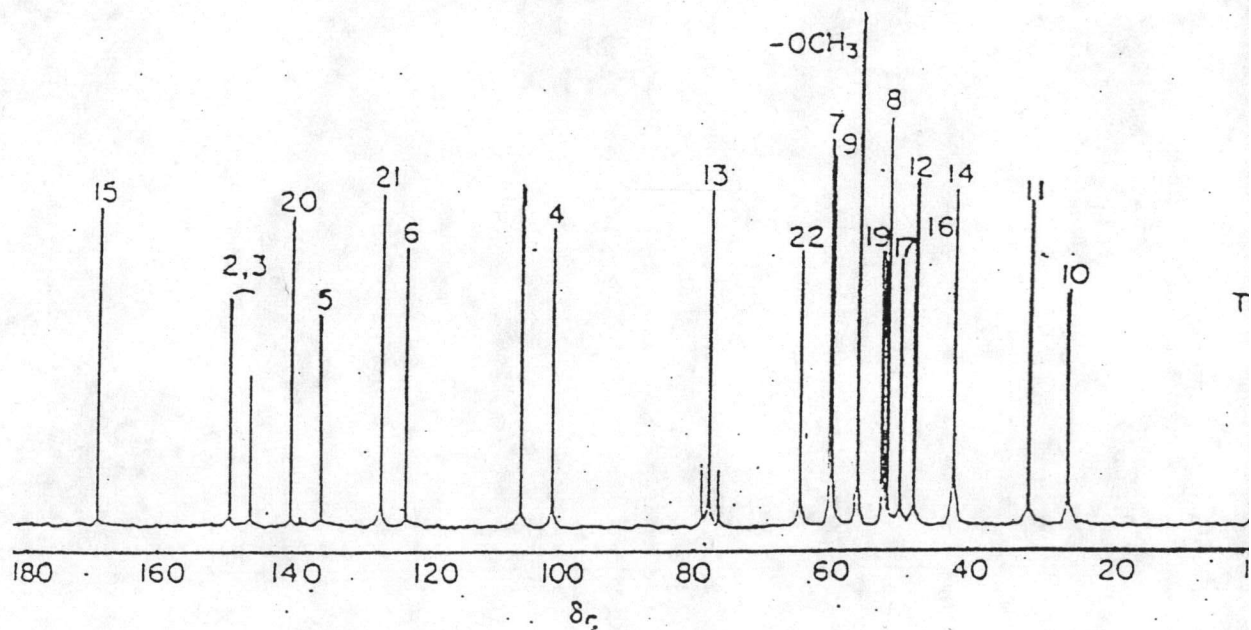
Figure 6   Proton noise-decoupled ^{13}C spectrum of Brucine.

1.2   Off-resonance decoupling, single-frequency off-resonance decoupling (SFORD) (17,18)

Off-resonance decoupling gives a simplified spectrum and also retains "residual" ^{13}C coupling information while removing the much smaller long range couplings. The result reduces the splitting J value. The off-resonance spectrum is possible to discriminate between methyl, methylene, methine, and quaternary carbons. From various patterns of the coupling, methyl carbon atoms appear as quatets, methylene as triplets, methine as doublets and quaternary carbon as singlet. The off resonance spectrum and proton noise decoupling of brucine is shown in Figure 7.

The graphical evaluation of SFORD spectra show correlation of carbon chemical shifts with their proton counterparts. A series of SFORD spectra is recorded by stepping the decoupler frequency in increments and the peak frequencies are subsequently plotted against the decoupler frequency. Since the intersections of the straight lines occurs at the exact resonance frequency of each of the protons, these points can now be correlated with the proton spectrum plotted on the coordinate. This is illustrated in Figure 8 for a series of SFORD spectra displaying the aromatic region in 6-methylcoumarine and this experiment unambiguously assigns the two closely C-3 and C-8.
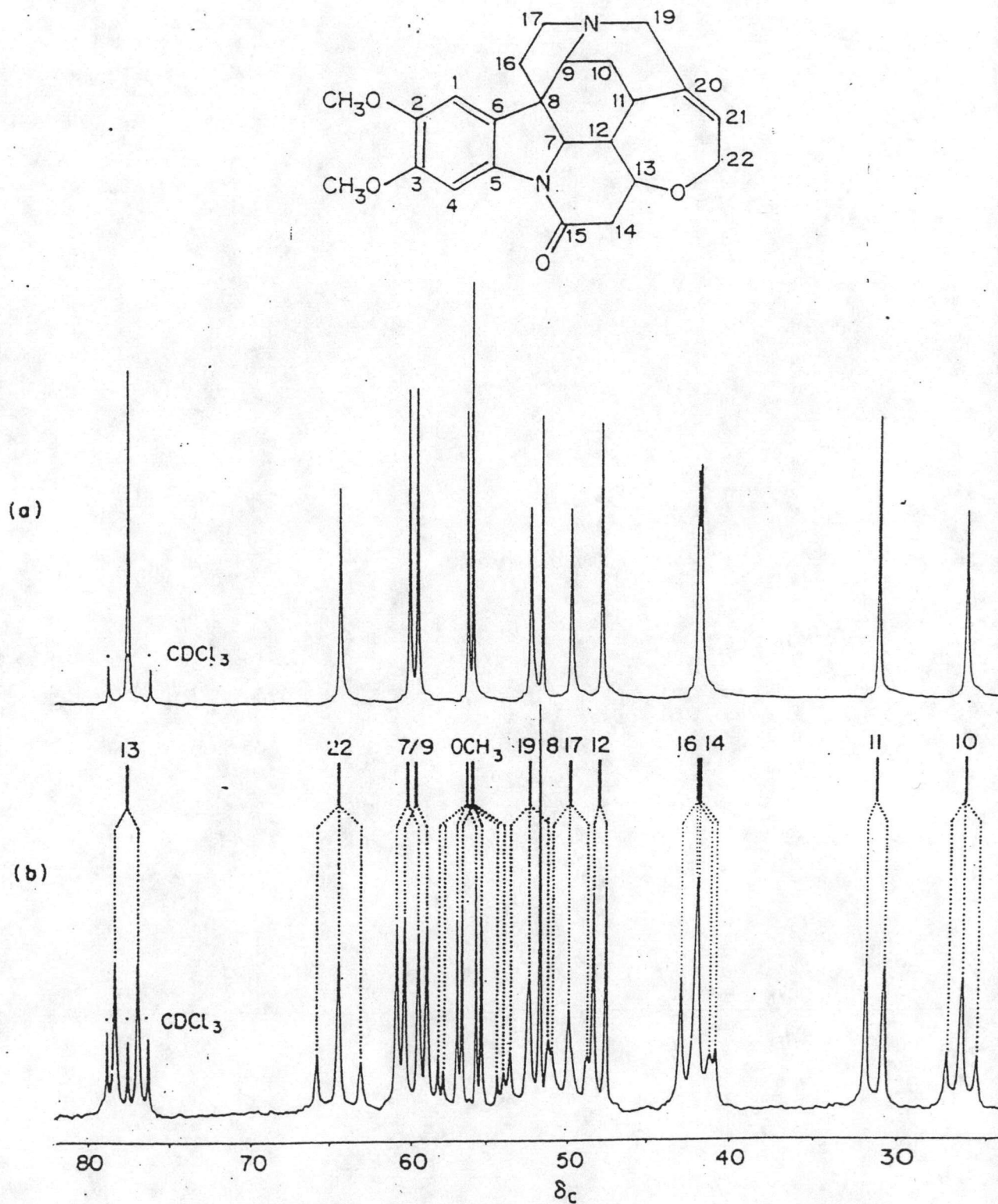
Figure 7 ^{13}C spectra showing the aliphatic carbon region of Brucine, (a) Proton-noise decoupled, (b) Off-resonance decoupled.
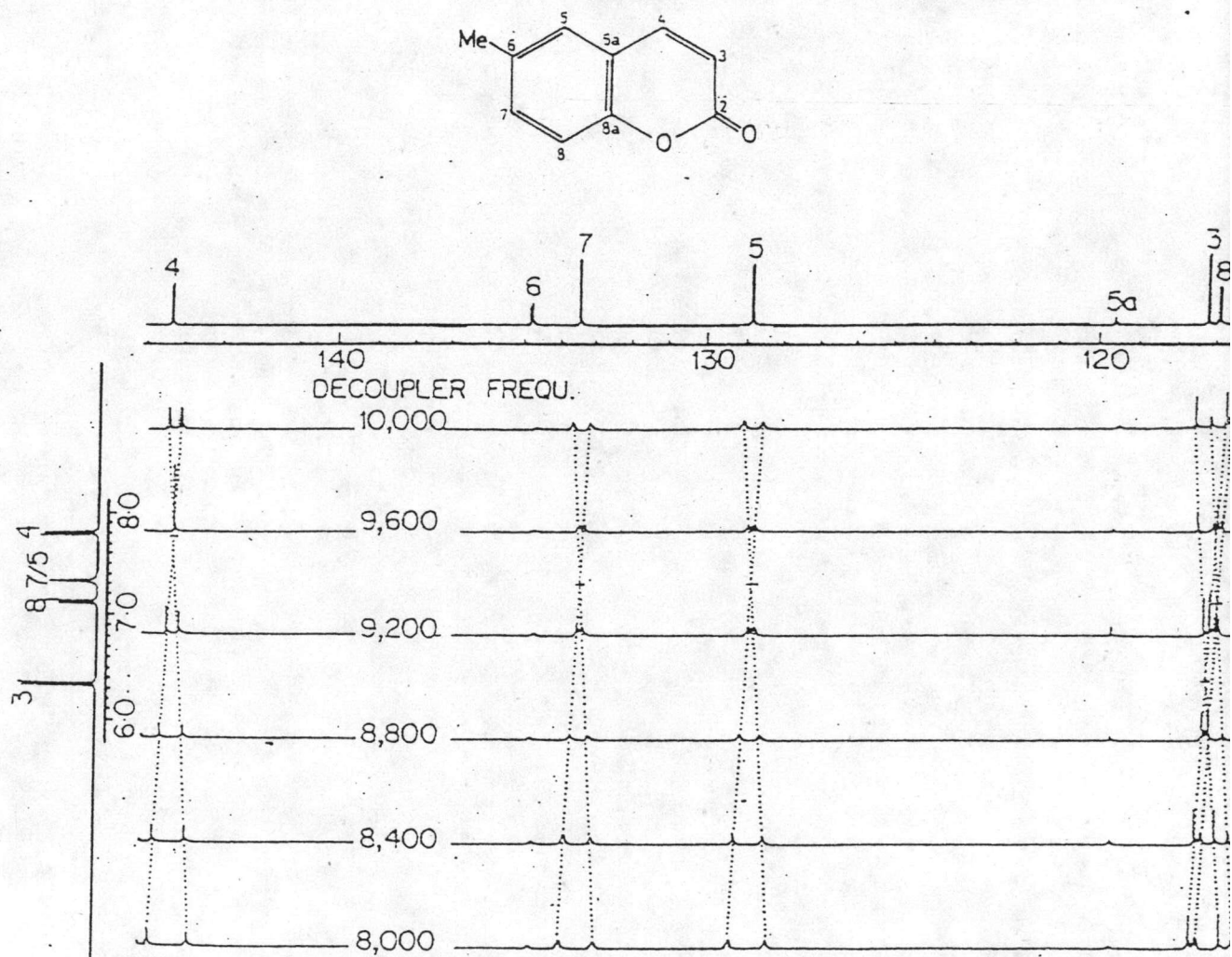
Figure 8   Series of ^{13}C SFORD spectra, showing   the
aromatic region in 6-Methylcoumarin.

This method does not only permit correlation of carbon chemical shifts with known proton shieldings but it may in fact be a method for identifying not directly observable protons in complex molecules where individual protons are masked by a broad signal envelope.

1.3 Selective proton decoupling (16)

The general purpose of the selective decoupling experiment is to establish a one-to-one correspondence between proton and carbon shieldings. When a specific proton is irradiated at its exactly frequency at a lower power level than the one used in off-resonance decoupling. This result is that the ^{13}C spectrum correlated directly to irradiated proton becomes a singlet, while the other ^{13}C spectra show residual coupling.

This technique has been used for peak assignment but satifactory results depend on finding the precise frequency of the proton and the appropriate power level for decoupling. Figure 9 shows such an array of selectively decoupled spectra obtained on the sample of 6-methylcoumarin.

1.4 NOE-enhanced proton-coupled carbon spectra (19)

In the experiment the transitions of proton are irradiated while the resonance of carbon is observed since the irradiating field is very strong. The proton decoupler is initially turned on during a pulse delay
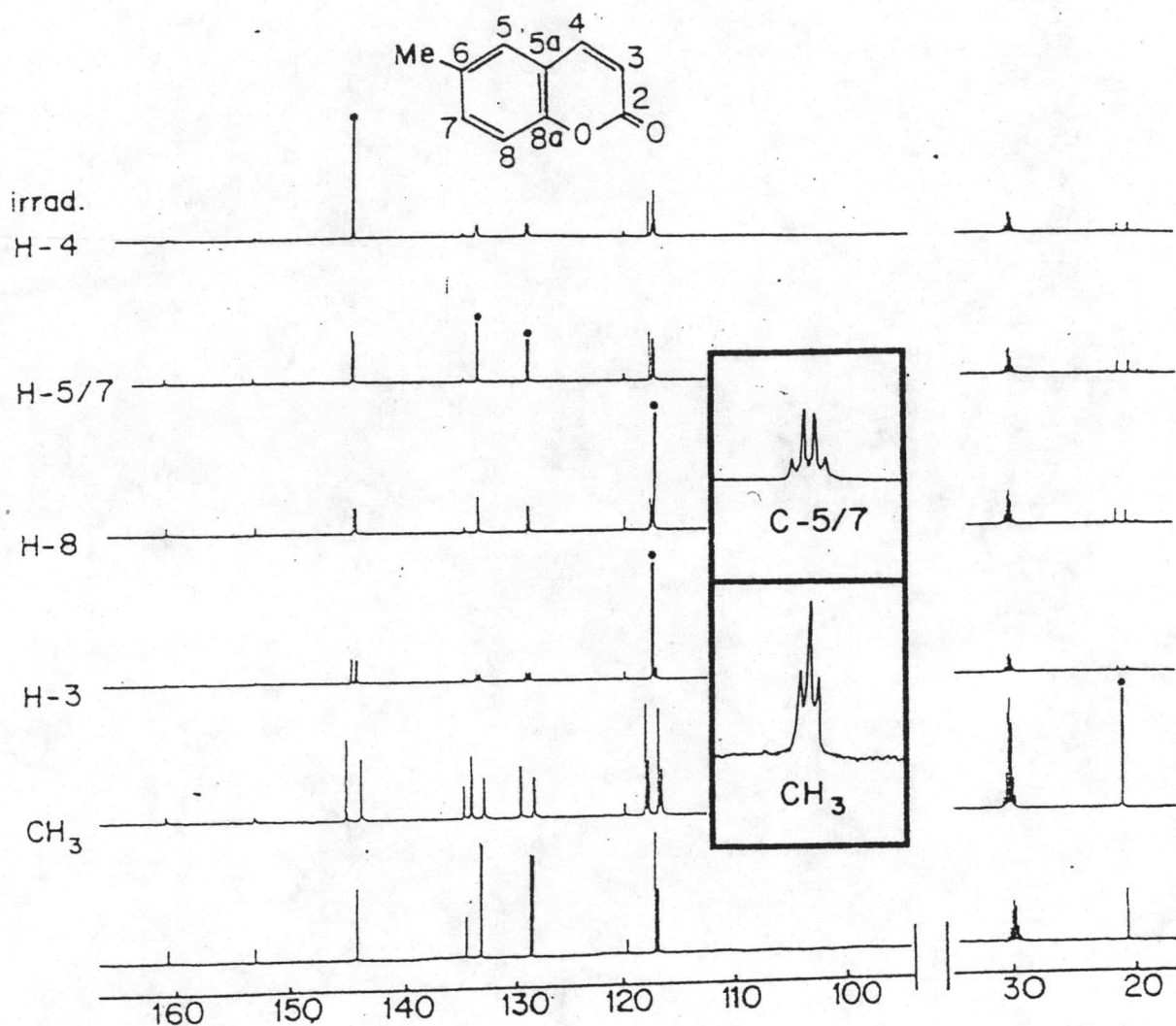
Figure 9   Array of selectively decoupled ^{13}C spectra of
6-Methycoumarin signals of fully decoupled
carbons in each trace are labelled with a
dot(.).

(PD), but turned off during data acquistion (AT) (Figure 10).

The objective of the experiment is showing obviously the coupling between proton and carbon atom and increasing the signal of spectrum. The gated decoupling technique can be used to measureue the ^{13}C-H long range coupling constant or line spliting (20). The long range ^{13}C-H coupling has been used for complex molecule assignment because the coupling interaction more than 2 bonds give the information that can identify the carbon atom in the different environment of molecule. Figure 11 shows the enhanced s/n of 2-bromoaniline spectrum achieved by this experiment.

1.5   Gate decoupling without NOE

This experiment is as same as in gate decoupling with NOE but the proton decoupler is turned on during a pluse, turned off during free induction decay (FID) to a pluse delay (PD) (Figure 12). As a result the ^{13}C spectrum has no effect of the NOE so, the intensity of the carbon signals depends on the number of carbon and we can calculate the area of signal by a electronic integrator. The area or intensity of each signal is the portion of the number of carbon of each signal so the gate decoupling without NOE spectra are used as a tool for quantitative analysis.

(a)
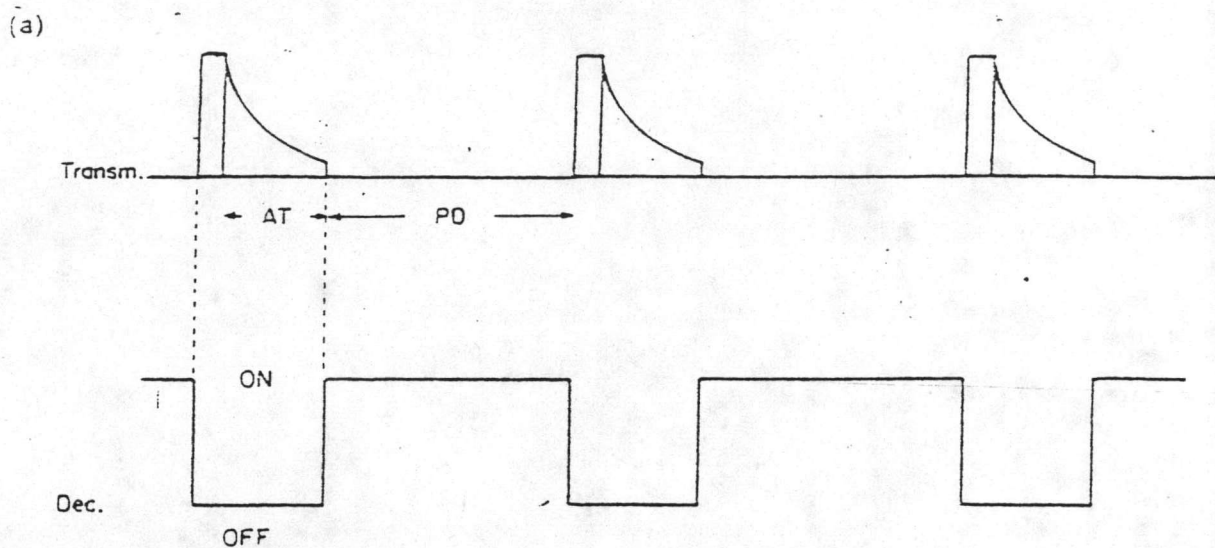
Figure 10   Timing diagram in a gated decoupling experiment.

(a)
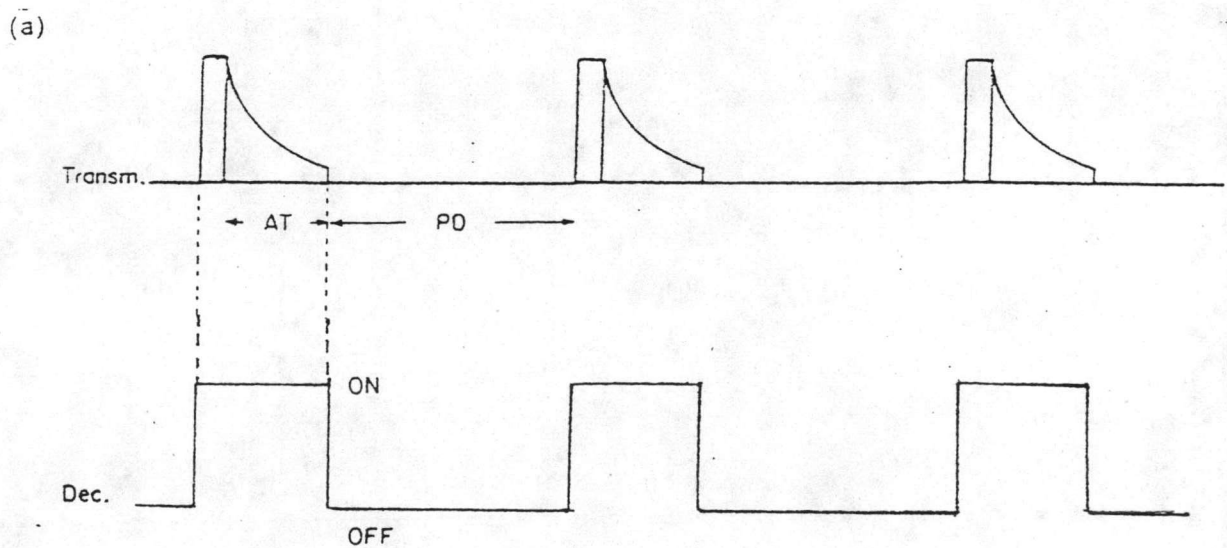
Figure 12   Timing   diagram   in a gated decoupling without NOE
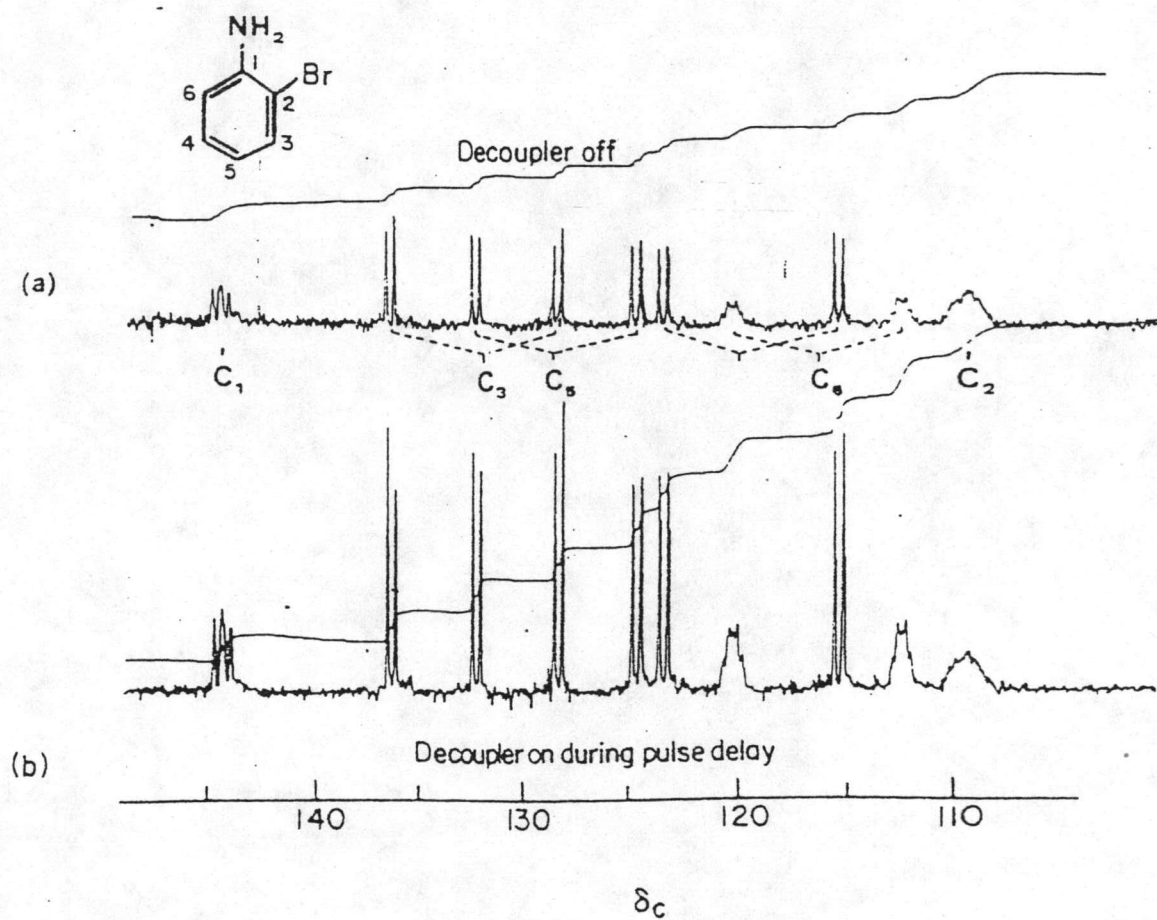
Figure 11   (a) Proton-coupled spectrum of 2-Bromoaniline,
             (b) Gated decoupling spectrum of 2-Bromoaniline.

2. Polarization transfer and related experiments

Polarization transfer is a double irradiation technique for increasing sensitivity and obtaining the multiplicity information. The physical commonality of the experiments is a ^{13}C polarization enhancement, induced by transfer of magnetization via scalar coupling from the proton to the ^{13}C spins. This can result in intensity enhancements of up to a factor r_H/r_C irrespective of the mechanism governing relaxation. The polarization transfer constitutes the basis for heteronuclear two dimensional correlated spectroscopy.

2.1 Selective Population Inversion (SPI) (21,22)

The principle of this experiment is to selectively invert the spin populations on the energy levels defining a proton transition. The resulting population change affects the intensities of those carbon transitions that share an energy level with those of the perturbed proton transition.

It is the easiest to discuss this in relation to the simple AX coupling system (A = ^1H, X = ^{13}C), whose interconnecting energy levels are shown in Figure 13a. The spin populations are designated in terms of the quantities $\Delta\alpha 1/2 \gamma H$ and $\delta\alpha 1/2 \gamma C$, providing the relative populations given in Figure 13 since in thermal equilibrium the spin populations are approximately proportional to the Zeeman energies. The transition

a)
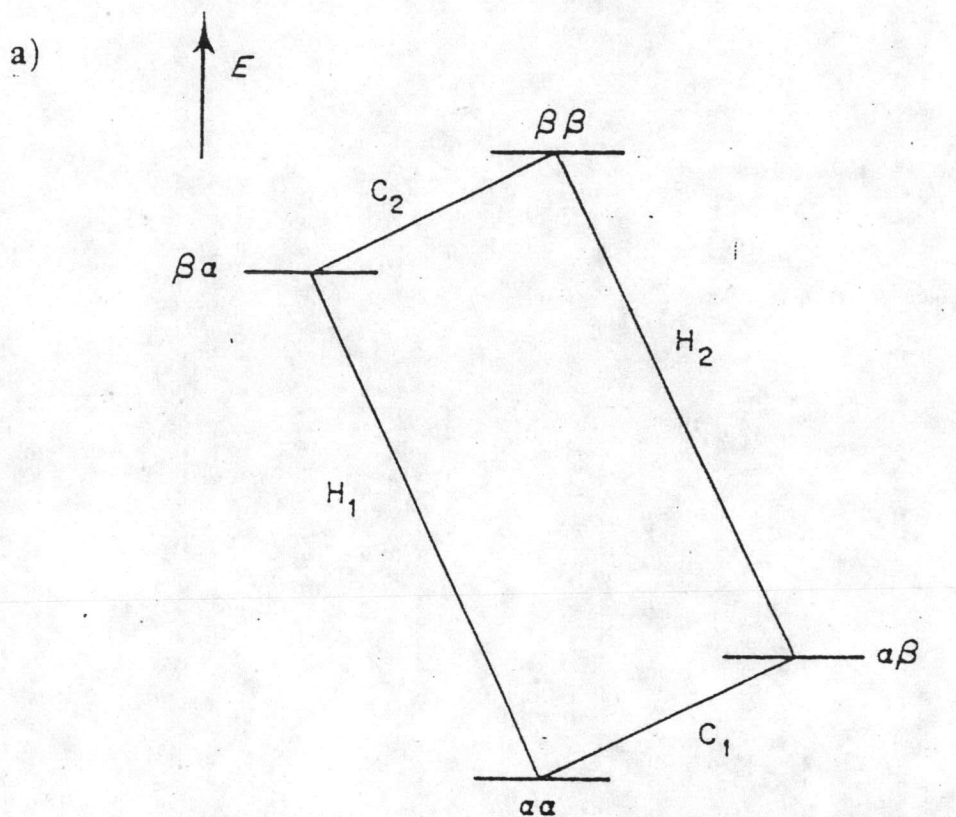
b)

Energy	Spin state	Spin population	
		a	b
$\frac{1}{2}\nu_C + \frac{1}{2}\nu_H$	$\alpha\alpha$	$\Delta + \delta$	$\Delta + \delta$
$-\frac{1}{2}\nu_C + \frac{1}{2}\nu_H$	$\alpha\beta$	$\Delta - \delta$	$-\Delta - \delta$
$\frac{1}{2}\nu_C - \frac{1}{2}\nu_H$	$\beta\alpha$	$-\Delta + \delta$	$-\Delta + \delta$
$-\frac{1}{2}\nu_C - \frac{1}{2}\nu_H$	$\beta\beta$	$-\Delta - \delta$	$\Delta - \delta$

[a] At thermal equilibrium.

[b] Following a 180° inverting pulse of H(2).

Figure 13   (a) Schematic energy level diagram for an AX spin system (A = ^{1}H, X = ^{13}C) allowed proton and ^{13}C transition are labelled H_1, H_2, and C_1, C_2, respectively.

(b) Energy states and relative spin population for the AX spin system.

intensities for 2 proton and 2 carbon transitions are proportional to the respective population differences, i.e. $I_{H(1)} = I_{H(2)} \alpha \Delta$. The selective 180° proton (decoupler) pulse inverts the populations between levels $\alpha\beta$ and $\beta\beta$ (H_2 transition). As a result the relative populations are given in the last column of Figure 13b and it is verified that the new populations become.

$$I_{H(1)} \; \alpha \; 2 \Delta \quad\quad I_{(C1)} \; \alpha \; 2 \Delta + 2 \delta$$
$$I_{H(2)} \; \alpha \; (-2 \Delta) \quad I_{(C2)} \; \alpha \; (-2 \Delta + 2 \delta)$$

The proton populations are tranferred to the carbon transitions, which experience a fourfold increase and a fourfold decrease, respectively, as seen if one takes into account the fact that $\nu H / \nu C \sim 4$, consistent with $\Delta = 4\delta$.

The SPI experiment can identify carbons which coupling to geminal and vicinal protons. An illustrative example is given in Figure 14, the spectra of oxaline (23). When C-8 proton (Figure 14b) is selectively inverted, C-10 and C-2 are affected both carbons couple to H-8 by vicinal coupling (Figure 14c), C-12 and C-13 are identified when C-15 proton is selectively inverted.

2.2 Insensitive Nucleus Enhancement by Polarization Transfer (INEPT) (16,21,24)

The major limitation on the applicability of the SPI technique is the utilization of selective pulse. The inversion pulse affects only one particular transition so
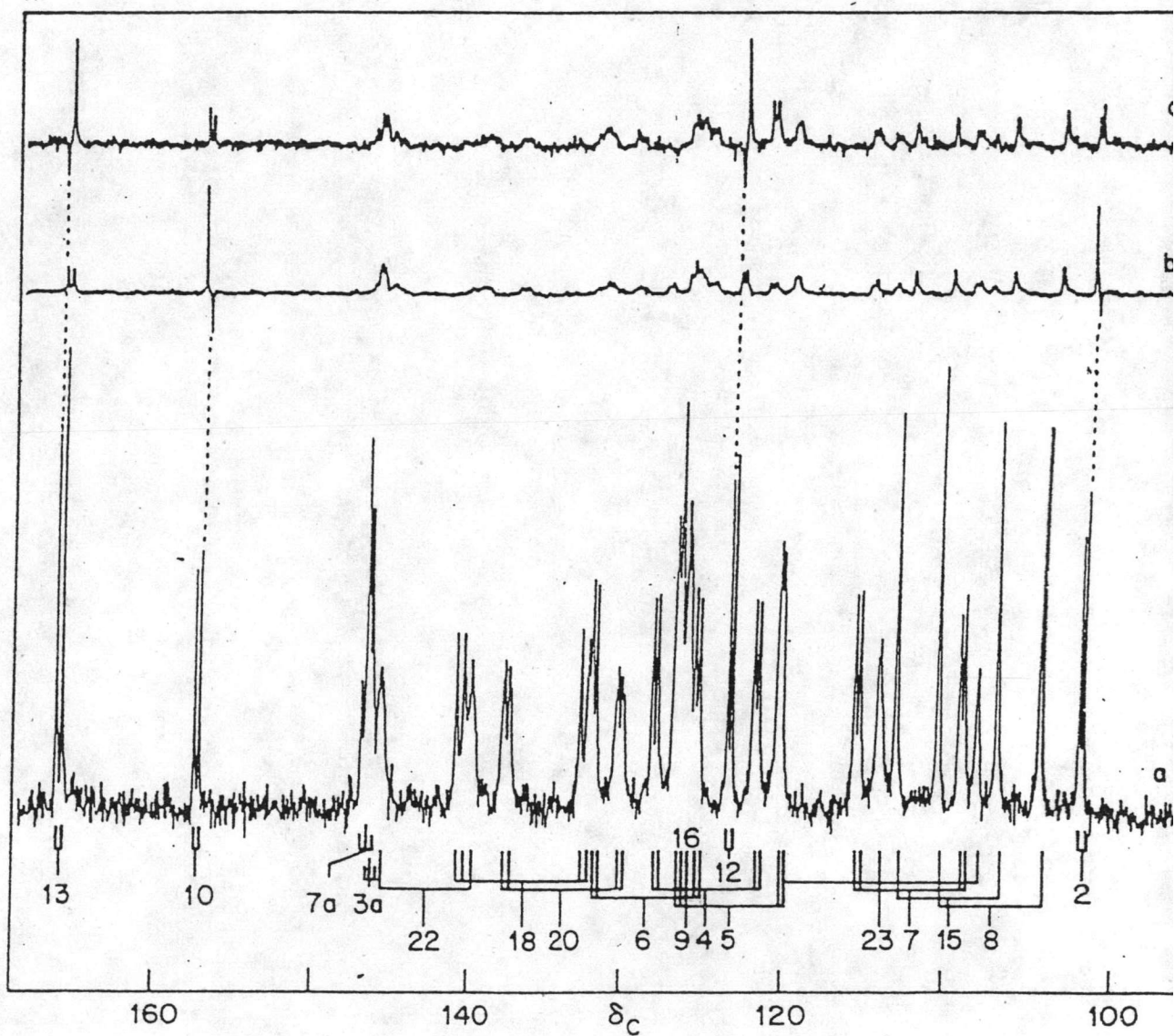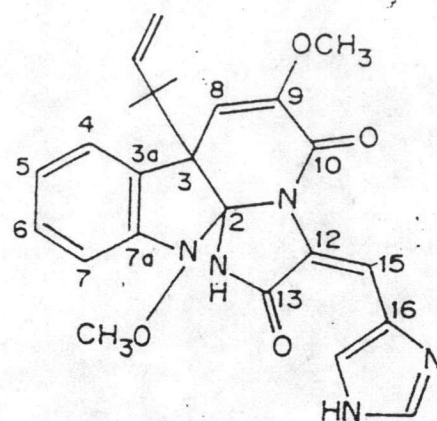
Figure 14 ^{13}C spectra of Oxaline,
(a) Proton-coupled,
(b) SPI experiment; transition of C-8 proton
selectiviely inverted,
(c) same as (b); Transition of C-15 proton
selectively inverted.

the SPI method lack of generality. The objective of the INEPT experiment is inversion of the populations on one of two proton transitions especially for all protons, independent of their chemical shift by using non−selective pulses. The principle of INEPT is to change the time parameter (τ) during the pulse sequence of sensitive nucleus (H) which coupled to less sensitive nucleus (C) in order to transfer polarization.

The INEPT experiment can be summarized in Figure 15, 16. (25). The starting point is a non-selective 90° decoupler pulse, the proton magnetization is aligned along the transverse plane (Figure 16a, 16b). T_1 is chosen such as to meet the condition $T_1 = (4J)^{-1}$ and relative phase angle (o) is $2 \pi J T_1$. During the following period T_1, the two proton magnetization components make up an angle of 90°, as illustrated in Figure 16c. A 180° proton pulse acting at time $t = \tau_1$ converts the two components into their mirror images (Figure 16d). A 180° carbon pulse is applied in synchronism with the refocusing proton pulse, this causes reversal of the spin states (Figure 16e). At time $t = 2T_1$, the two components $M_{H(2)}$ align along-x´ and x´, respectively (Figure 16f). A 90° proton pulse converts $M_{H(1)}$ and $M_{H(2)}$ into longitudinal plane (Z plane) (Figure 16g). This corresponds with the desired antiphase polarization of the doublet, so 90° carbon pulse elicits an enhanced response as in SPI. The proton-coupled INEPT spectra are illustrated in Figure 17.
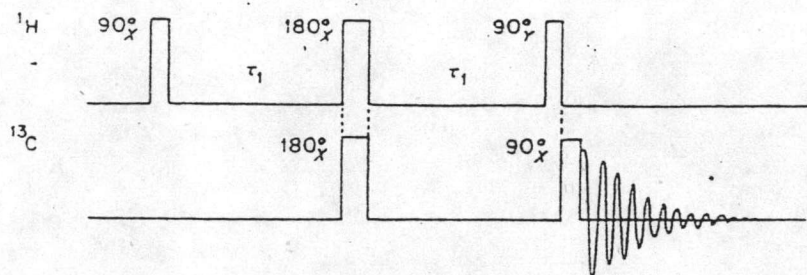
Figure 15   The pulse sequence of INEPT experiment.
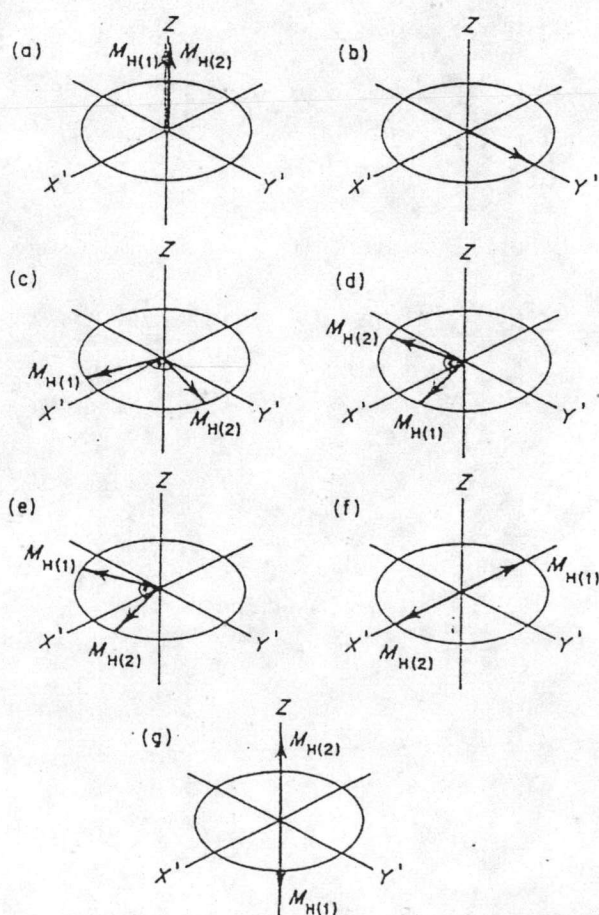
Figure 16   Behaviour of the proton magnetization shown for $^{13}C^1H$ (AX spin system) during an INEPT in the rotating frame.
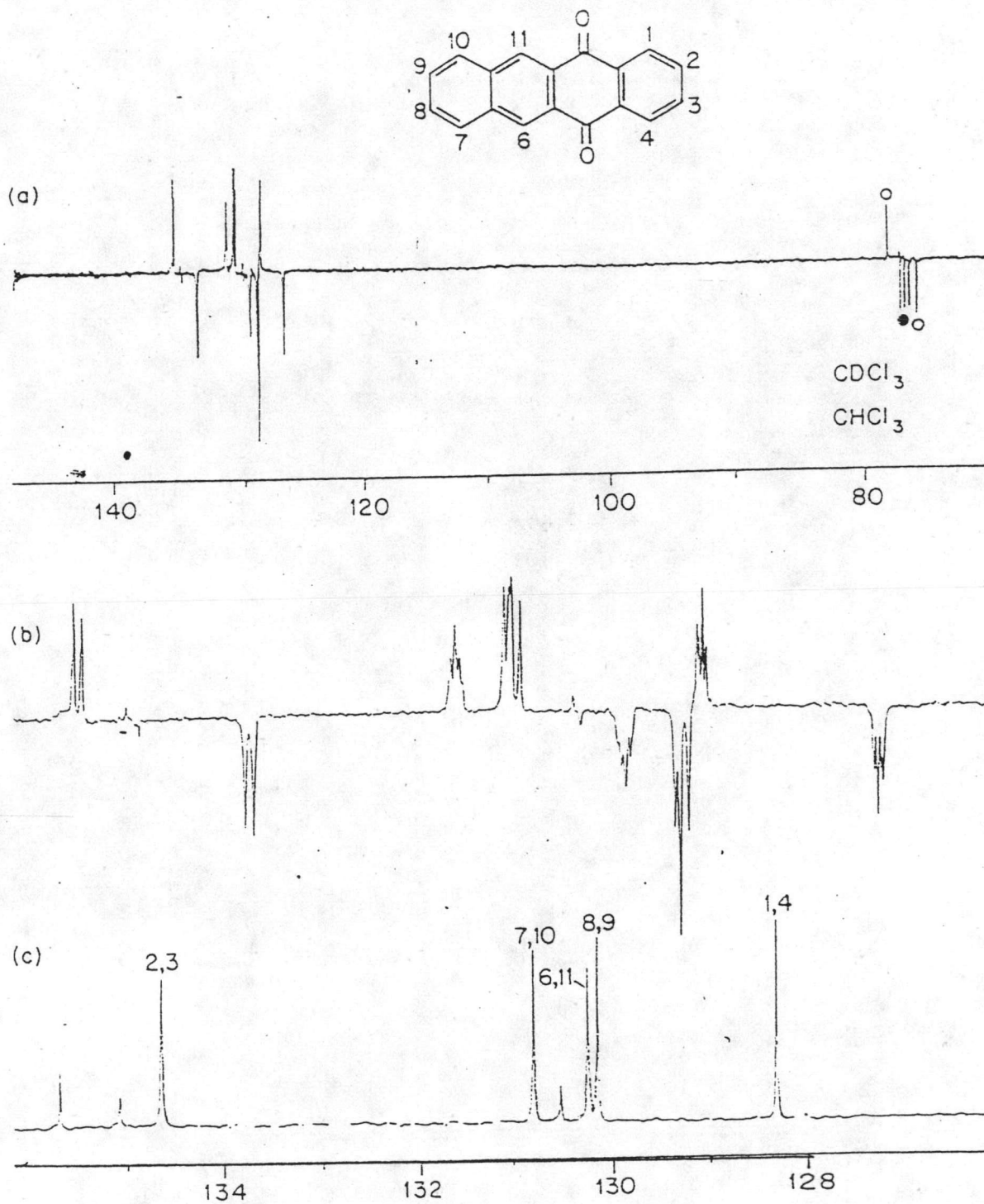
Figure 17   (a) Proton-coupled ^{13}C INEPT spectra of the aromatic region of Naphthacene quinone.
(b) Expanded spectrum.
(c) Proton noise-decoupling spectrum.

A basic INEPT spectrum cannot be acquired with proton decoupling, because of the antiphase disposition of the components of multiplets. The simplest remedy to this problem is to introduce a delay between the 90° read pulse and the beginning of acquisition. The purpose of this delay is to allow for spontaneous rephasing of antiphase multiplet components. More effective refocusing is achieved by applying a 180° spin echo pulse at the midpoint of the period ($\Delta/2 = \tau_2$) to both ^{13}C and ^{1}H spins, as shown in the timing diagram Figure 18. This modification of the basic polarization transfer experiment is sometimes referred to as "INEPT with refocusing and decoupling" (26,27). The extent of polarization transfer is related to the two time periods τ_1 and τ_2 and to multiplicity of the signal. The dependence of the enhancement factor E on the refocusing period τ_2 is plotted in Figure 19, calculated according to EQNS. 1-3, assuming $\tau_1 = (4j)^{-1}$

$$E_{CH} = (\nu_H/\nu_C) \, SIN(2\pi J \tau_1) \, SIN(2\pi J \tau_2)$$

$$E_{CH} = (\nu_H/\nu_C) \, SIN(2\pi J \tau_1) \, SIN(4\pi J \tau_2)$$

$$E_{CH} = (3\nu_H/4\nu_C) \, SIN(2\pi J \tau_1)$$
$$\{[SIN(2\pi J \tau_2)] + SIN(6\pi J \tau_2)\}$$

It is the evident that there is no value of τ_2 which optimizes the signal enhancement for all three spin configurations. For example in Figure 19, the condition $\tau_2 = (4J)^{-1} (2\pi J \tau_2 = \pi/2)$ both CH_3 and CH_2 signals are suppressed, whereas $\tau_2 = (2.7J)^{-1} (2\pi JT_2 = 3/4\pi)$
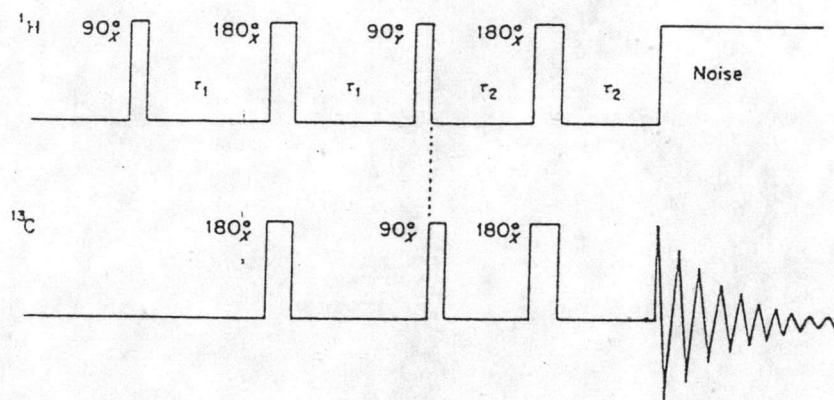
Figure 18   The pulse sequence of INEPT with refocusing and decoupling.
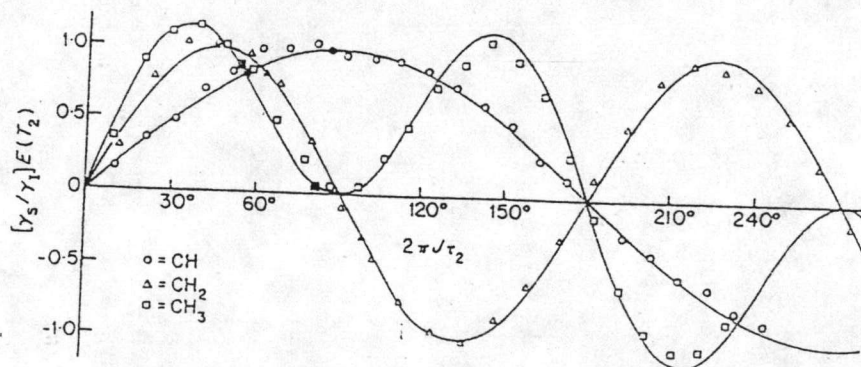
Figure 19   Dependence of the enhancement on the phase angle (ϕ) ϕ = 2π J T$_2$ for CH (circles), CH$_2$ (triangles), and CH$_3$ (squares) signal for an INEPT experiment.

affords positive signals for CH and CH_3 but inverted for
CH_2.   This behaviour is illustrated with the spectra of
lasalocid (Figure 20).

2.3 Attached Proton Test (APT) (16,28)

The technique strictly does not belong to the
category of polarization transfer experiments because the
attached proton test (APT) pulse sequence does not entail
any transfer of polarization from protons to ^{13}C. On the
other hand, it is a simple method for determining
multiplicity in the fully decoupled recording mode.

The principle of APT is to let the spins precess
during a delay period following an initial non-selective
90° observation pulse. During this free precession period
the magnetization components, characterized by the various
spin states of the attached protons, build up a relative
phase angle, determined by the magnitude of ^1JCH and
multiplicity. Figure 21 shows the evolution of the
tranverse ^{13}C magnetization for the three spin systems,
^{13}CH, $^{13}CH_2$, and $^{13}CH_3$. It is evident that at the time t
$= J^{-1}$ the magnetization components are realigned for all
three coupling situations. The phase of the methine and
methyl signals is opposite to that of the methylene
signals. Not shown in the figure is the behaviour of
quarternary carbons which are unmodulated and give rise to
the same relative phase as the methylenes. The timing
diagram of refocusing APT is shown in Figure 22.
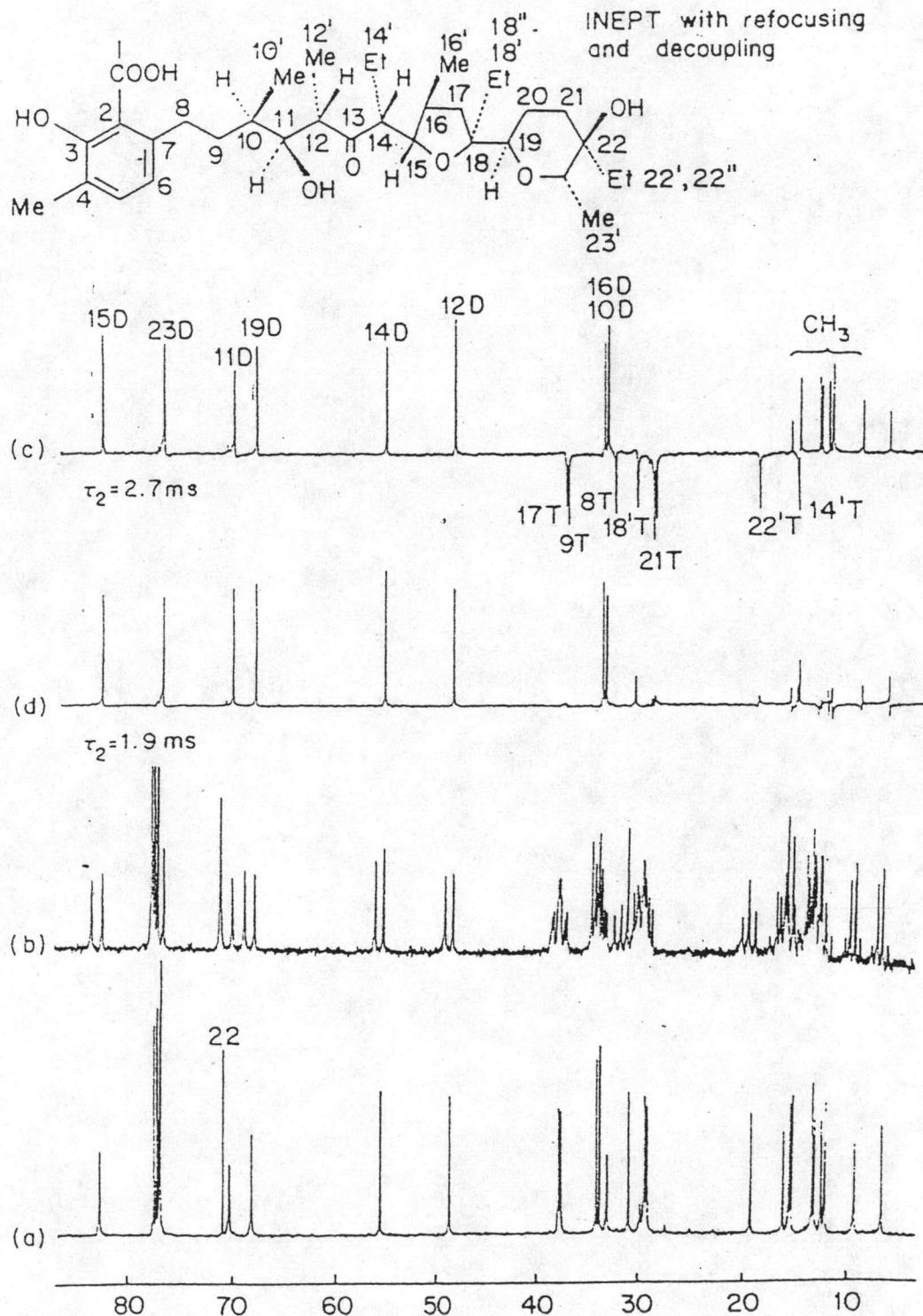
Figure 20 ^{13}C spectra of the aliphatic region in Lasalocid
(a) Proton noise-decoupled,
(b) SFORD,
(c), (d) INEPT with refocusing and decoupling,
(c) $T_2 = (2.7\ J)^{-1}$: CH$_1$, CH$_3$ > 0, CH$_2$ < 0 < (d)
$T_2 = (4\ J)^{-1}$: CH$_3$, CH$_2$ = 0, CH > 0.
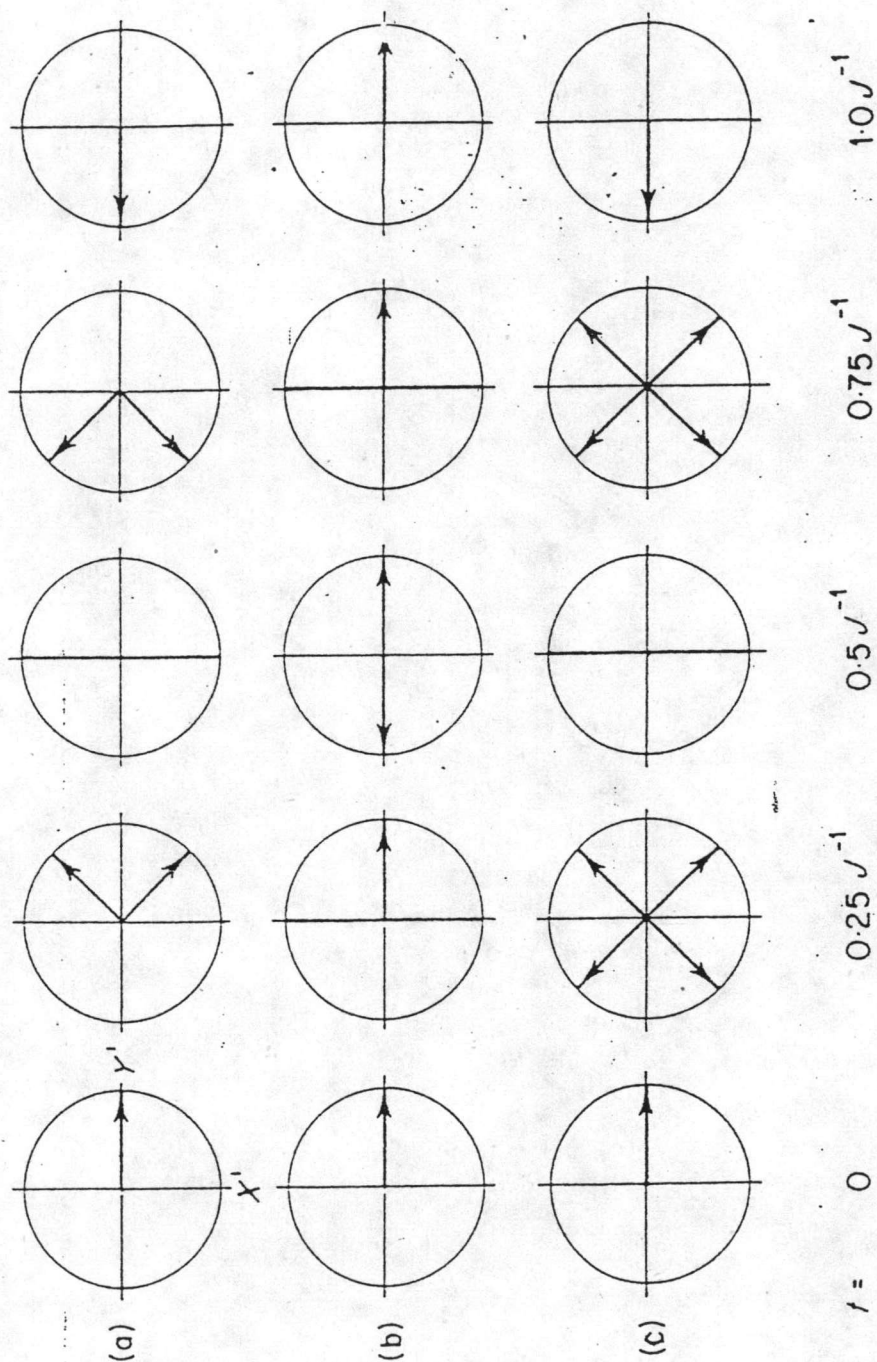
Figure 21 Evolution of the transverse ^{13}C magnetization, following a 90° pulse, for the three spin systems ^{13}CH (a), $^{13}CH_2$ (b) and $^{13}CH_3$ (c).
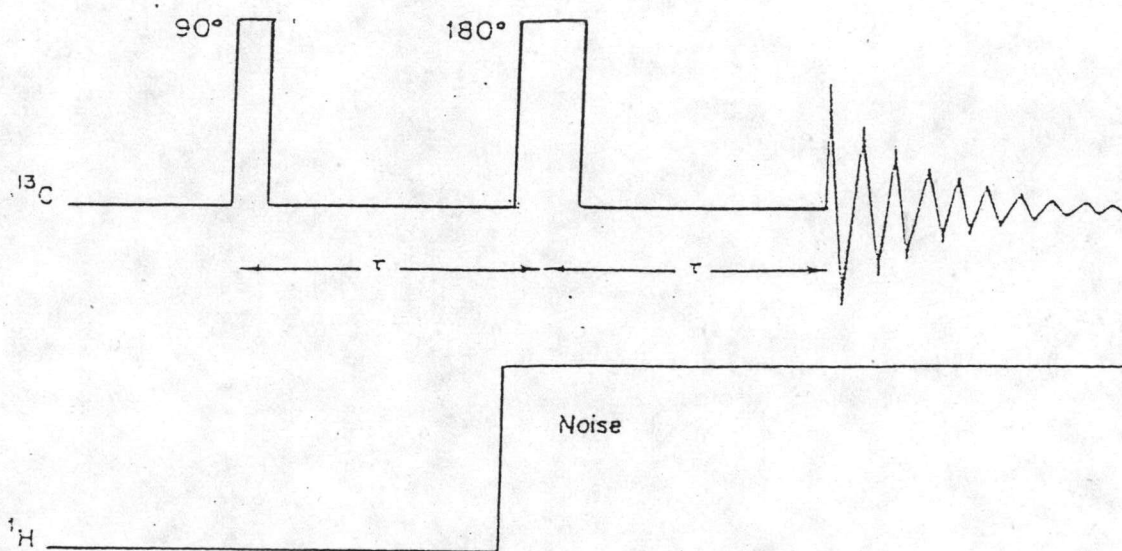
Figure 22   The Attached Proton Test (APT) pulse sequence.

APT is definitely not quite as a powerful method as INEPT for multiplicity selection since it does not permit distinction between CH and CH_3 and it lacks the benefit of sensitivity enhancement. However, it is shown the quaternary signals. On the other hand, it is simple to implement and does not require sophisticated instrumentation. Figure 23 illustrates the application of the refocused APT technique for multiplicity determination in strychnine.

2.4 Distortionless Enhancement by Polarization Transfer (DEPT) (29,30,31)

The DEPT experiment brings about polarization transfer in a similar fashion to INEPT. The important difference is the variation of the final proton pulse angle and all the signals of the insensitive nucleus are in-phase at the start of acquisition. Thus, decoupled spectra can be acquired without the need for an extra refocusing period. The sequence of DEPT can be summarized in Figure 24. (16) is set to $(2\tau)^{-1}$. The signal intensity as a function of various angles is plotted in Figure 25 for typical methyl, methylene, and methine resonances. It is obvious from Figure 25 that by taking intensity-weighted linear combinations of spectra collected with θ = 45°, 90°, and 135°, subspectra pertaining to a particular multiplicity can be obtained. For example, $\theta = 90^o$ provides CH only, $\theta = 135^o$ affords positive signals for CH, CH_3 but inverted for CH_2.

Figure 23   Proton noise-decoupled ^{13}C spectra of Strychnine
(a) Standard spectrum,
(b) Spectrum obtained by APT techique.
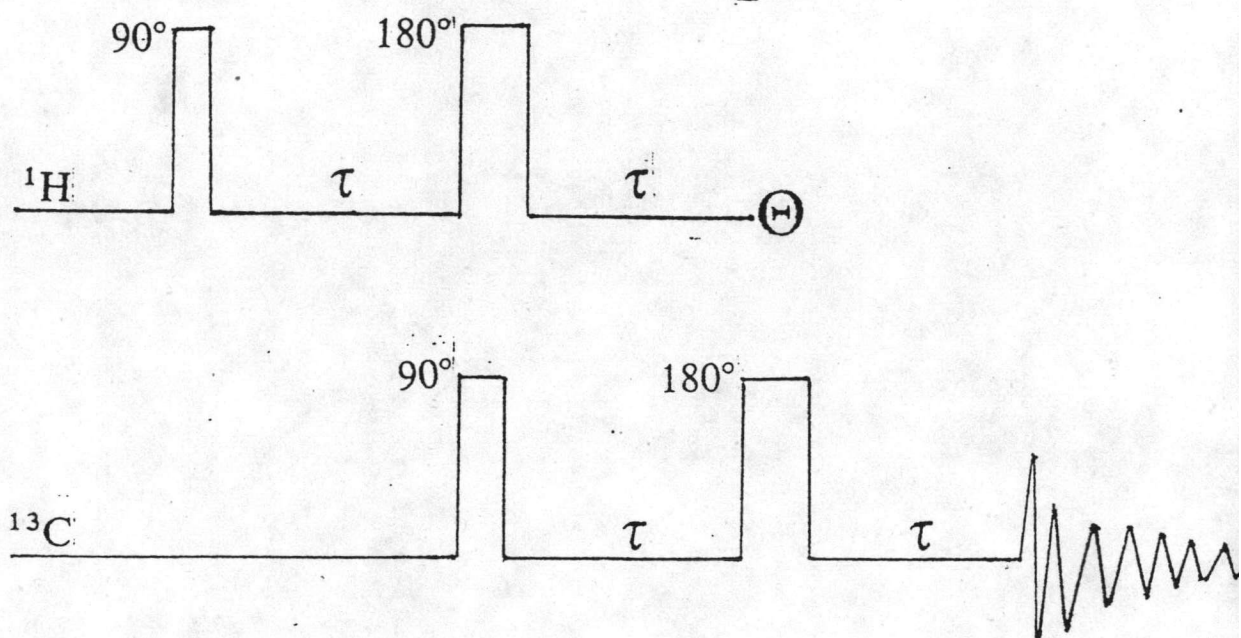
Figure 24   The pulse sequence of DEPT experiment.
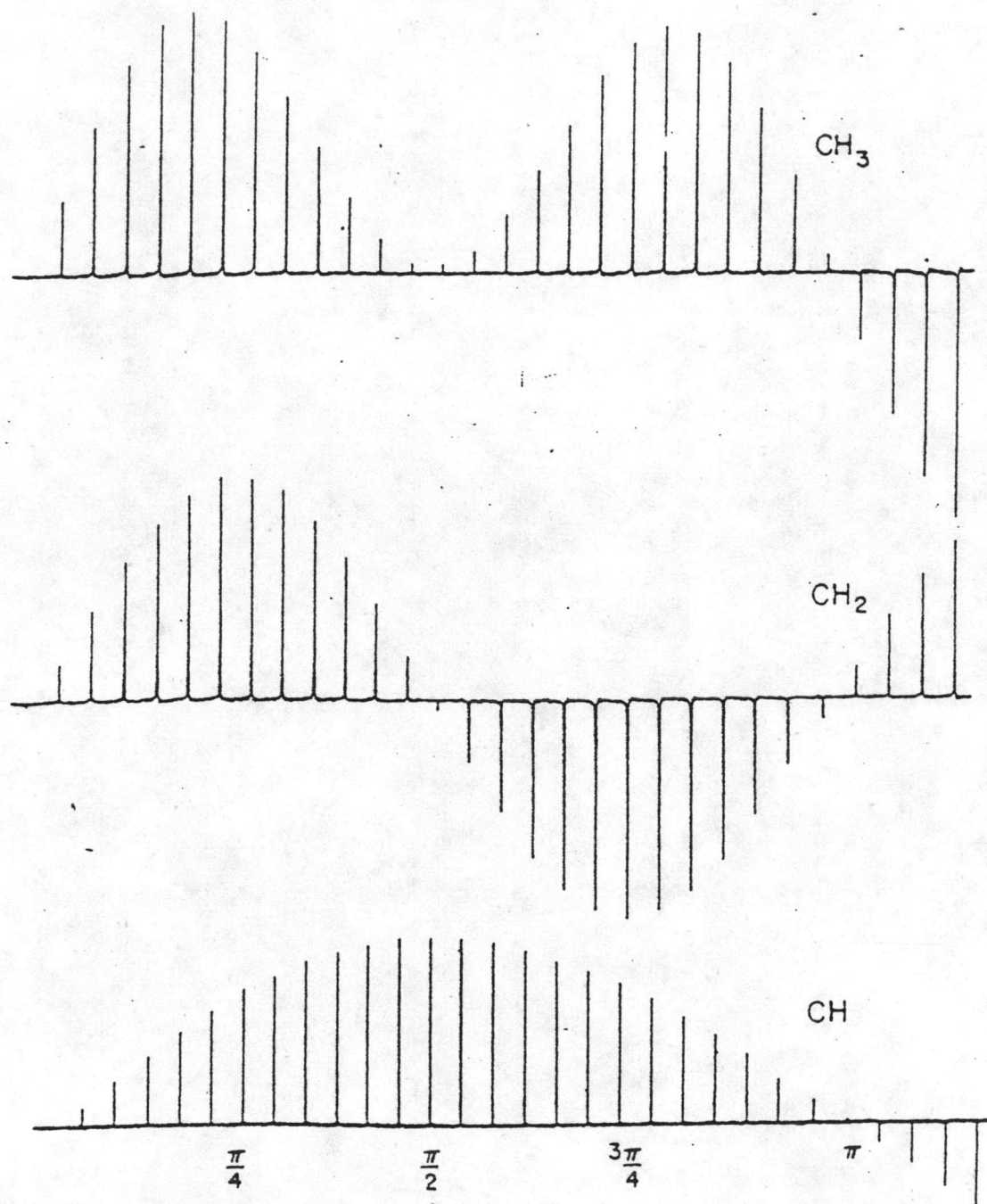
Figure 25   Proton-decoupled ^{13}C DEPT signals obtained with $\tau = (2J)^{-1}$ and various flip angles.

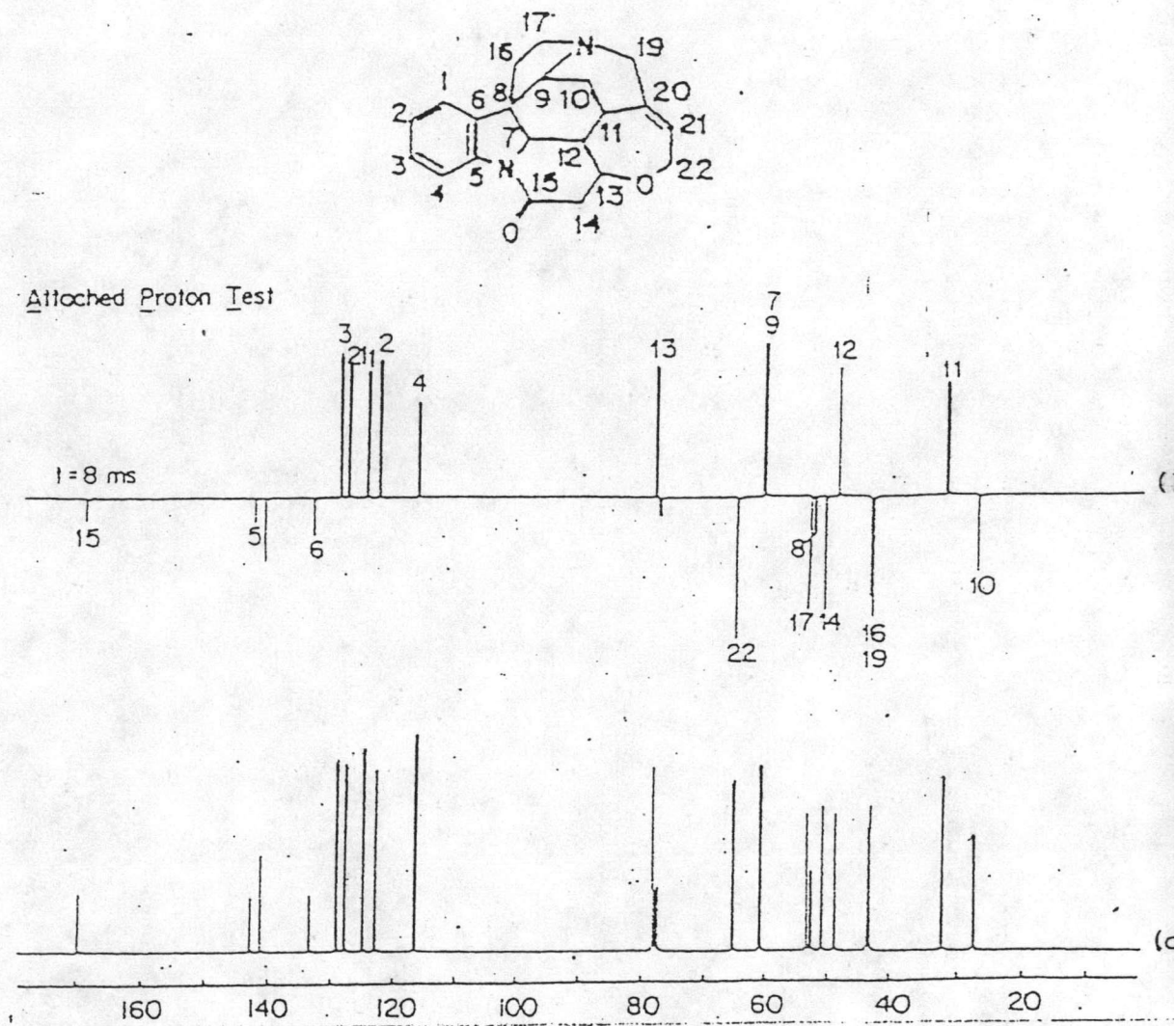The advantage of the DEPT technique is that the multiplet components are not distorted, therefore lending itself to decoupling. The DEPT experiment provides an alternative means for multiplicity.

3. Two-Dimensional Nuclear Magnetic Resonance (2D-NMR) (32,33,34,35)

The common feature of the 2D-NMR experiments is the time sequence as shown in Figure 26 (16,36) and the data are initially collected as a function of two time variables t_1 and t_2. During the preparation period the spin system is prepared in a suitable way. During the evolution period, characterized by a time variable t_1, the spin system evolves in a way specified by the purpose of the experiment. During the detection period t_2, finally, the data are acquired by the usual method, affording a FID in which every point is a function of both, t_1, and t_2. By collecting mFIDs, each differing in the value of t_1, starting with $t_1 = t$, and ending with $t_1 = m$. Δt_1, a time domain data matrix s (t_1, t_2) is obtained. Assuming each FID to consist of n data can be fourier-transformed twice, i.e. with respect to t_2 and t_1. As a consequence, two frequency variables F_1 and F_2 are also obtained:s (F_1, F_2).

There are two options available for presenting 2D spectra (32). One is the stacked plot (Figure 27). The second, and generally more preferred, option is the

Figure 26   Schematic   representation   of   the   three   time
periods in two-dimensional experiments.
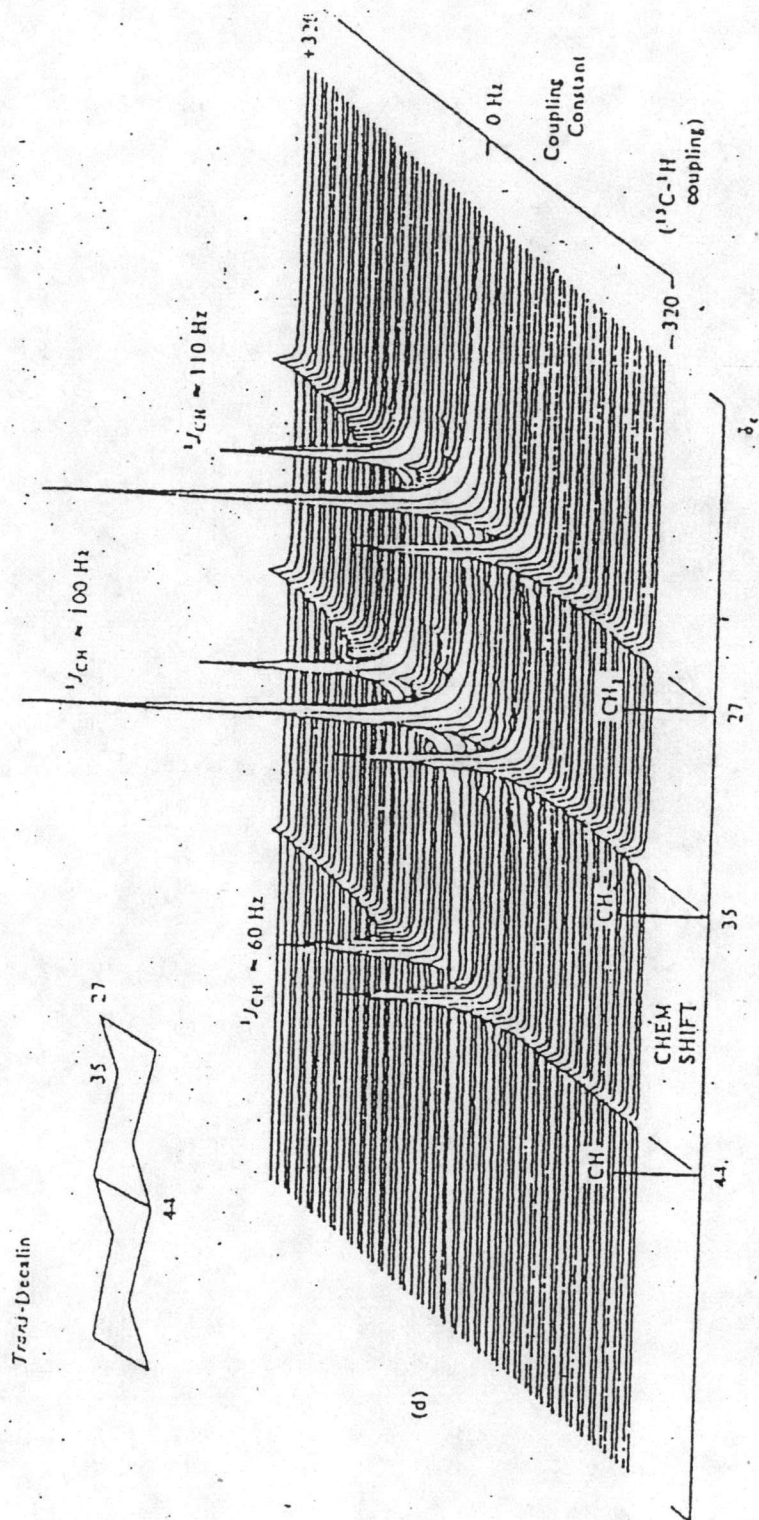
Figure 27   The 2D NMR stacked plot of trans-decalin, hetero-J resolved.

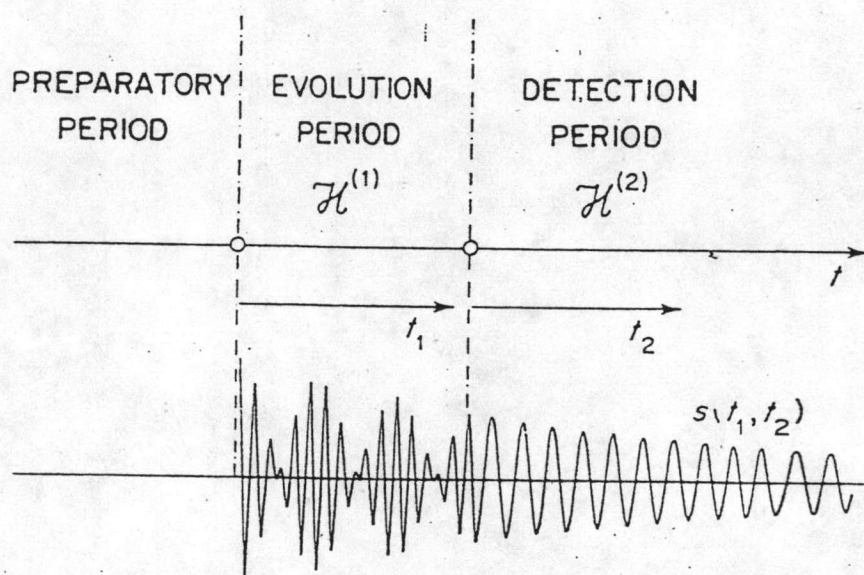contour plot which gives a top view of the data surface by taking a cross section through a stacked plot a chosen height (Figure 28).

There are generally two types of 2D experiment : these are called `J-resolved´ and `correlated spectroscopy´

3.1 J-Resolved Spectroscopy (37,38)

The J-resolved experiment is characterized by one frequeacy axis (F_1) containing scalar coupling information and the other (F_2) axis containing chemical shift information. The objective of using this technique is the resolution of all the J or scalar couplings. This technique may be used on both homo-and heteronuclear systems, but although it is more widely applied to the homonuclear case due to the ability to seperate overlapping multiplets. The heteronuclear J-resoved case is both a useful experiment for the measurement of $^{13}C...^{1}H$ couplings in complex spin systems and is also very easy to visualize.

The pulse sequence of heteronuclear case most commonly used is the gated decoupler method except that the fixed delay time T is replaced by the variable delay time t_1. Thus t_1 is varied in steps during the experiment (Figure 26) (24). In the heteronuclear case spin decoupling is normally applied at the proton resonance frequency during the acquisition period, and the resultant

Figure 28 ^{13}C NMR spectrum of 4-Methyl piperidine
(a) ^{1}H decoupled 1D spectrum,
(b) Contour diagram of the J (^{13}C, ^{1}H) resolved
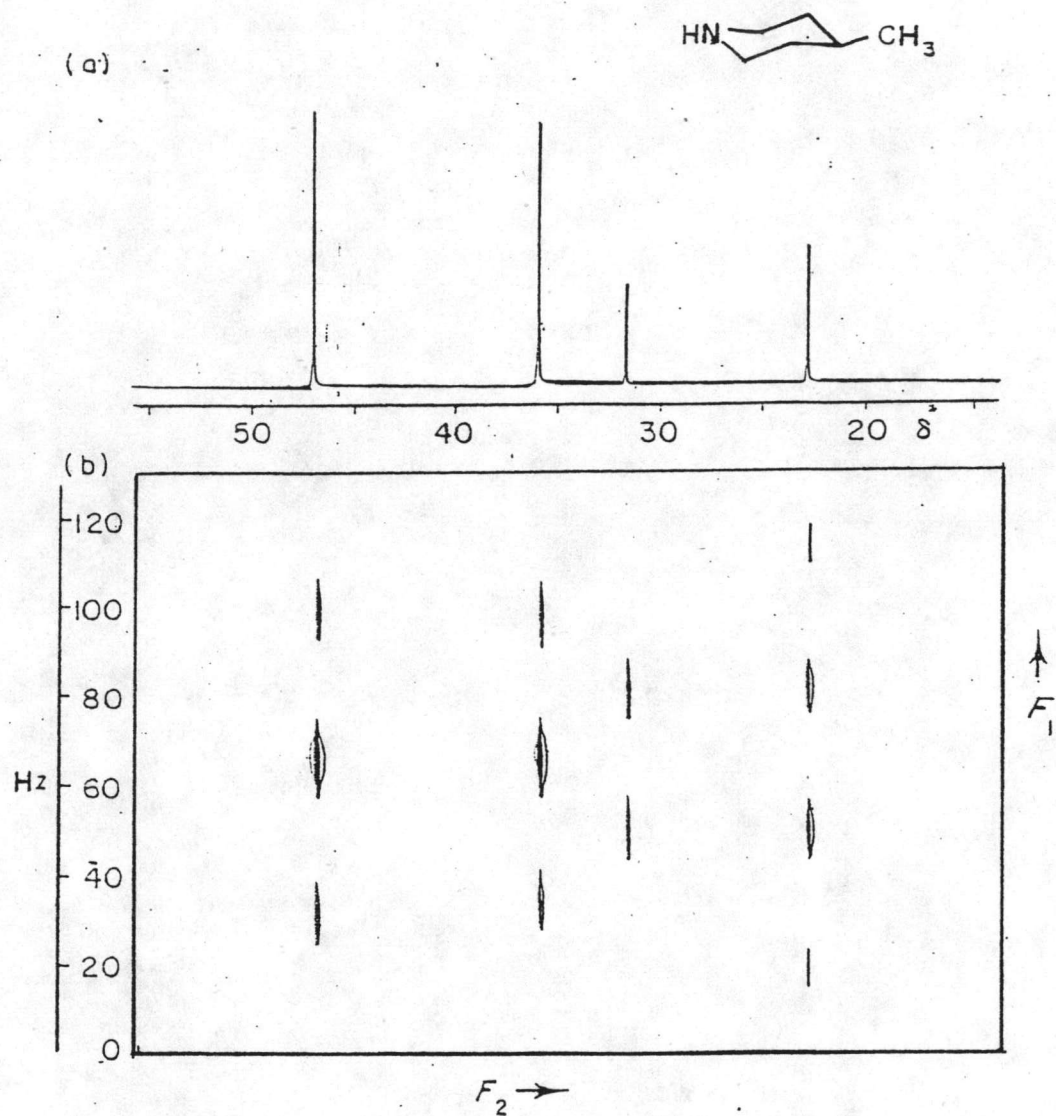2D spectrum.

2D spectrum then simply consists of, in F_2, the proton decoupled ^{13}C spectrum, and in F_1 the coupling constants J $(^{13}C \ldots ^1H)$. The illustrative example of this technique is shown in Figure 27, 28 (32).

In the homonuclear J-resolved experiment the pulse sequence is different, as broadband decoupling is replaced by the simple spin-echo sequence (Figure 29) and the delay time t_1 is again varying during the experiment, then it gives again a t_1-dependent signal as the heteronuclear case. In the homonuclear $(^1H \ldots ^1H)$ case the resultant 2D spectrum then simply consists of chemical shifts along F_2 to give a `proton decoupled´ proton spectrum and coupling constants along F_1. The example of application of this experiment is shown in Figure 30,31 (32,33).

3.2   Homonuclear shift correlation (21,32,33)

Correlated 2D NMR is the most common and easily used of the 2D techniques. It may be applied to both heteronuclear and homonuclear spin systems. The basis of the COSY (Correlated Spectroscopy) experiment is the process of coherence transfer in which magnetization is transferred between coupled spins. In the homonuclear experiment where $^1H-^1H$ spin-spin couplings provide the means for the transfer of magnetization and the nuclear spins are always coupled, therefore coupling information may always be transferred from one spin to another.
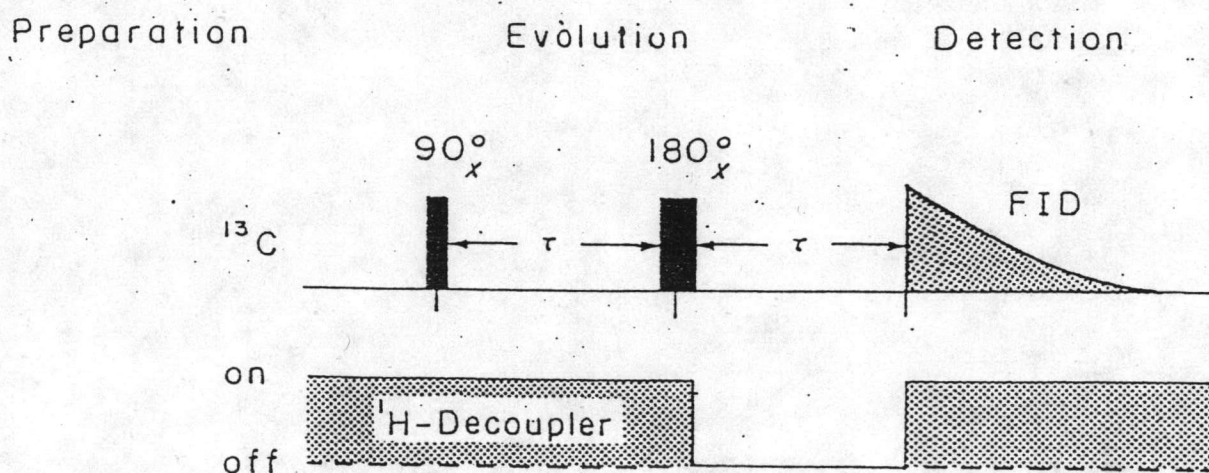
Figure 29   The SEFT (spin-echo Fourier transform) pulse
sequence.

(a)

(b)

(c)

F_1

$F_2 \rightarrow$

3   2   1   8
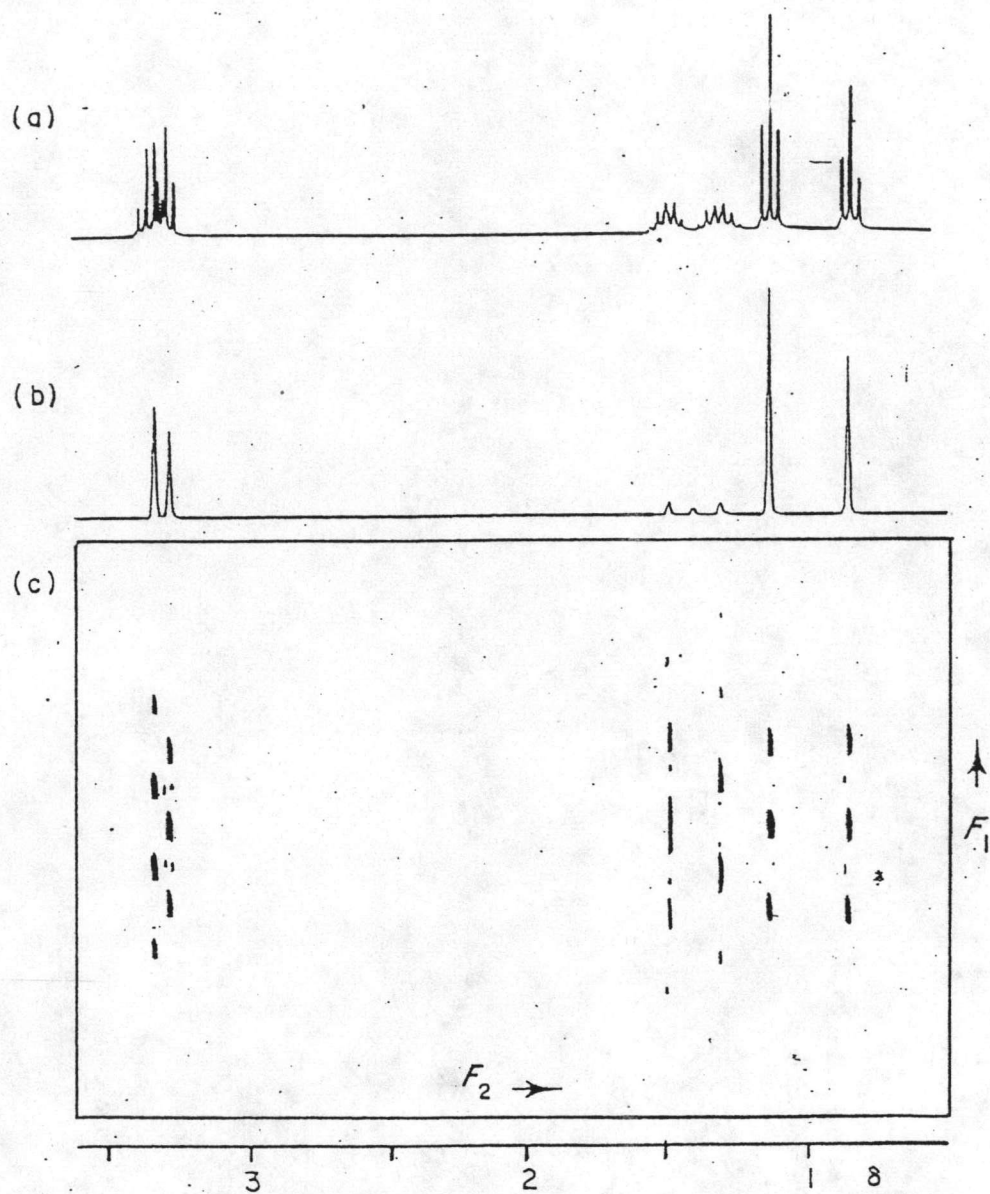
Figure 30   (a) ^{1}H spectrum of ethyl n-butyl ether.
              (b) The projection of the H-spectrum onto the
                   F_2-axis.
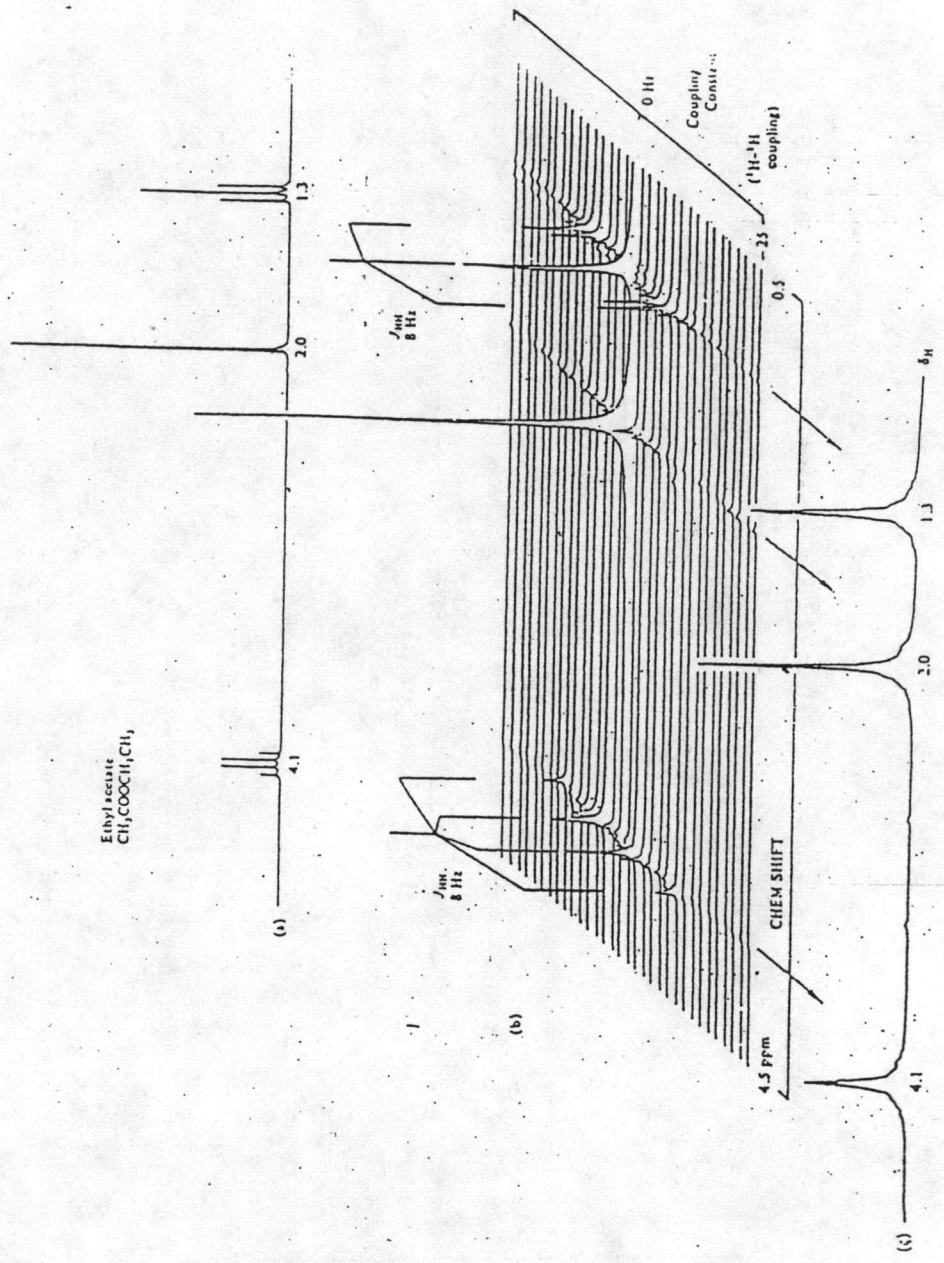   (c) The homonuclear J-resolved contour plot.

Figure 31   The 2D NMR stacked plot of Ethyl acetate, homo-J resolved.

The H-H COSY experiment consist of two 90° pulse seperated by a time period t_1 (Figure 32a) and the result of performing this experiment for the a nucleus of an AX spin system (A and X both protons) may be explained as follows. The initial 90° pulse causes the magnetization being flipped into x'y' plane. This second 90° pulse results in coupling information being transferred between the spins of the X and A nuclei. The 2D spectrum of the spin-coupled AX system, therefore, consists of the diagonal peaks (δ_A, δ_A), (δ_X, δ_X) and also of off-diagonal (or cross) peaks with coordinates (δ_A, δ_X), (δ_A, δ_X) (Figure 32a). These off-diagonal peaks indicate that A is indeed spin coupled to X. This spectrum (Figure 32b) is an example of the usual COSY contour plot in which the absolute value of the signal S (F_1, F_2) is displayed. This is the usual display mode for most 2D plots each proton appears at its approptiate position on the diagonal. In addition, however, there are off-diagonal peaks, caused by spin-spin coupling between two protons. To identify the chemical shifts of two coupling protons it suffices to draw a horizontal and a vertical line through a cross peak. The intersections with the diagonal locate the chemical shifts of the coupling protons.

An example of A H-H COSY contour plot is shown in Figure 33, which also gives the 1D proton spectrum of the compound 3-heptanone along both the F_1 and F_2 axis (32). This is a convenient method of displaying the COSY

a) Preparation │ Evolution │ Detection

b)

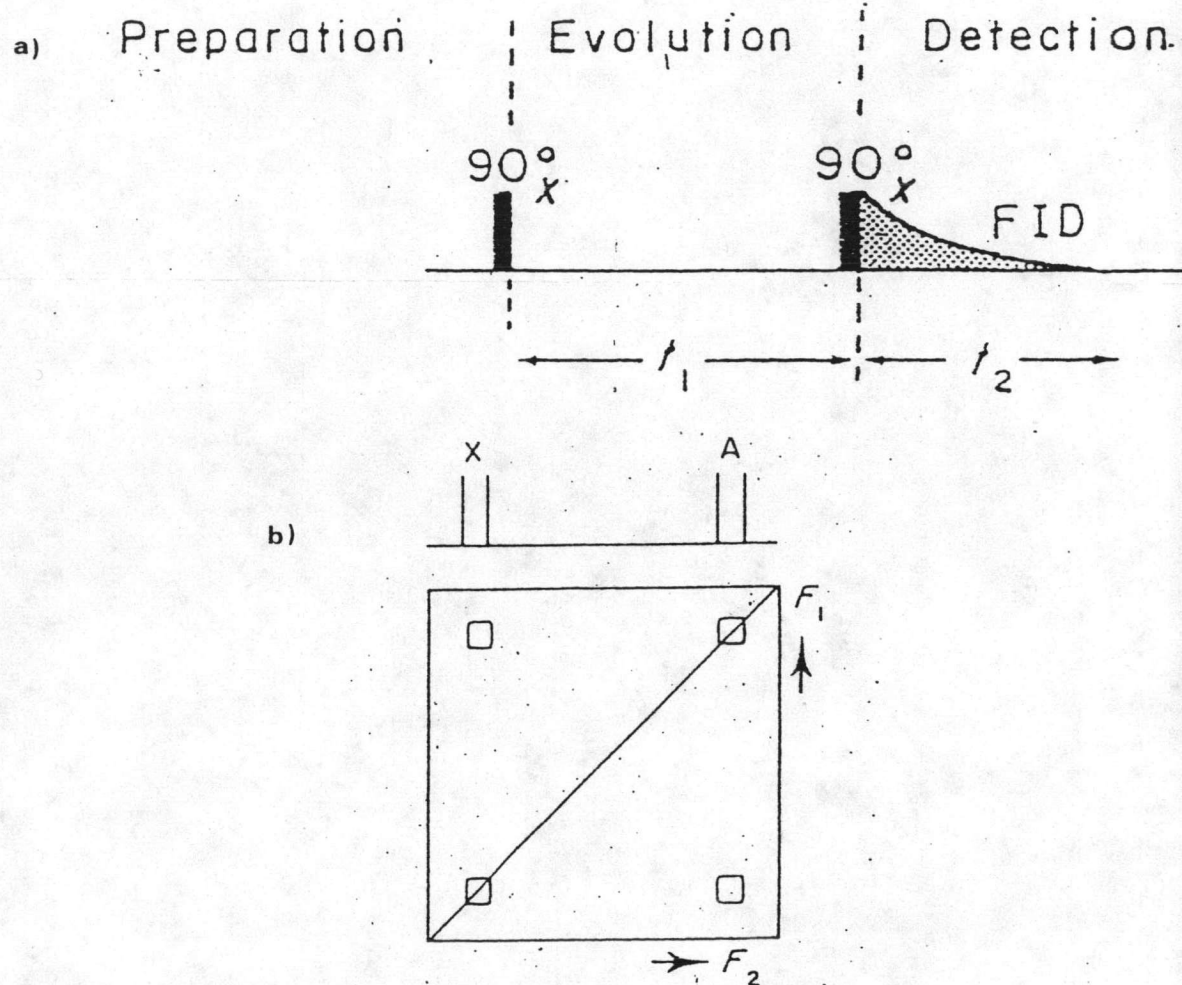Figure 32   The correlated spectroscopy experiment
             (a) Pulse sequence for the homonuclear case,
             (b) 2D absolute value mode contour for the AX
             case.

plots, as the diagonal and cross-peaks can be easily distinguished by inspection.

3.3 Heteronuclear shift correlation (39,40)

The heteronuclear correlated 2D experiment, especially for $^{13}C/^{1}H$ coupled systems, has also proved very useful. In this experiment one-bond $^{1}H-^{13}C$ couplings are used and therefore this experiment shows directly which protons are attached to which carbon atoms (the F_2-axis containing ^{13}C chemical shifts and the F_1 axis containing ^{1}H chemical shifts). The experiment is performed in a similar manner to the H-H COSY experiment. However in the heteronuclear case, more specially the $^{13}C/^{1}H$ case, broadband decoupling is used to acquire the FID during t_2. Because of this, prior to the detection period, an additional delay (called the 'mixing' time, $\Delta_1 + \Delta_2$) is required to permit the transfer of information between the ^{13}C and ^{1}H spins.

The pulse sequence of the heteronuclear case for an AX system (A = ^{1}, X = ^{13}C) is shown in Figure 34 (32), in which the ^{13}C nucleus is observed with broadband decoupling of ^{1}H. The initial 90° pulse on the ^{1}H nucleus rotates the spin vectors in to the x'y' plane. During the interval t_1 the proton magnetization precesses at a rates determined by the proton transmitter offset. The effect of the second proton pulse, whose purpose is to rotate the transverse magnetization M_{xy} back onto the Z axis, depends
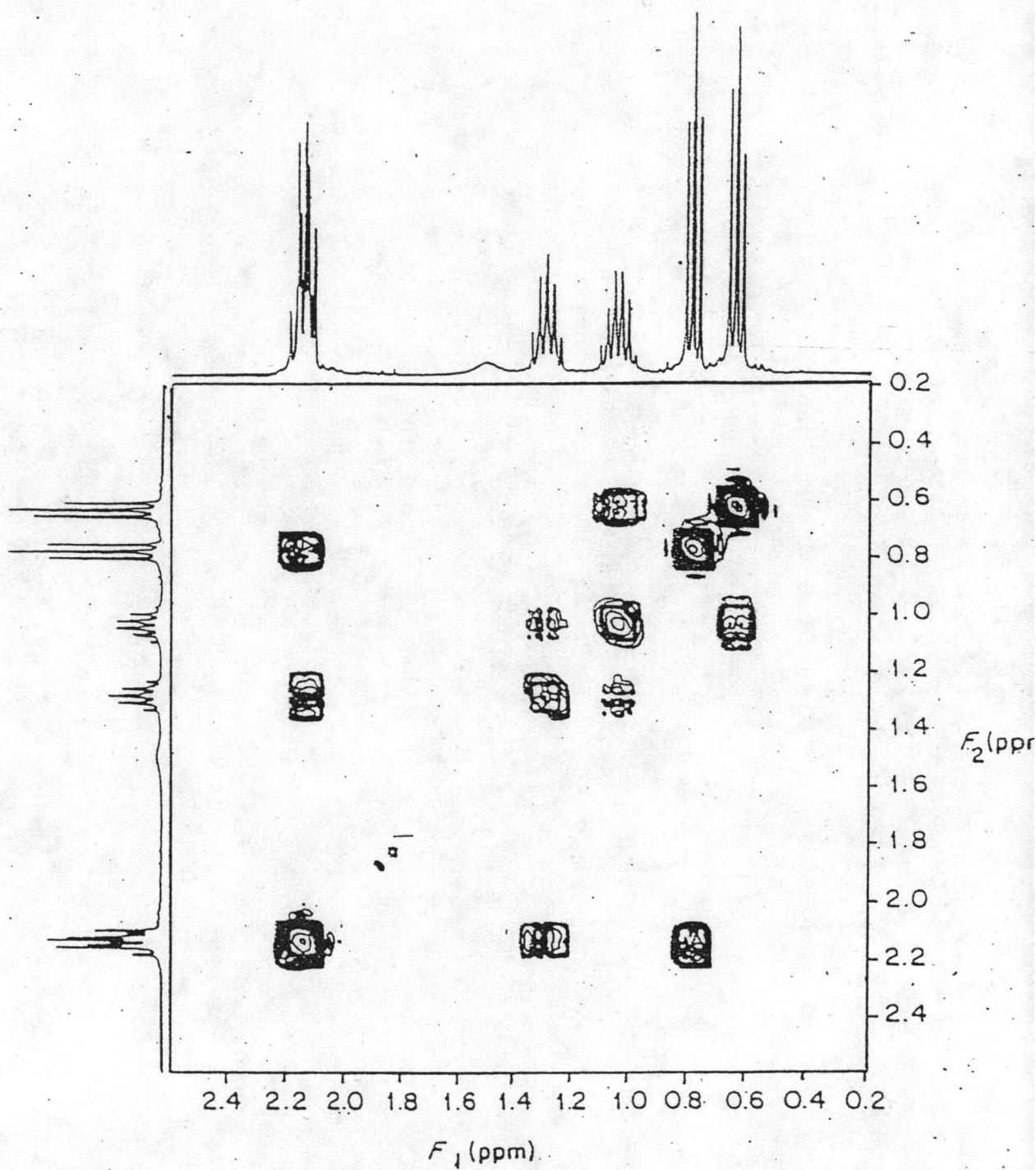
Figure 33   The ^{1}H spectrum and COSY contour plot   of   3-
Heptanone.

on the relative phase angle o of M_{xy}, only the y component is affected by the pulse. The phase angle o is a linear function of the time interval t_1. Immediately following the second proton pulse, a 90° ^{13}C detection pulse generates FID, carrying with the proton chemical shift as an amplitude modulation. The experiment is repeated m times by varying t_1, the evolution period of the experiment. A second fourier transformation in the t_1 dimension then provides a two-dimensional array in which the projection onto the F_1 axis represents the proton chemical shift. Both proton and carbon spectra are complicated by heteronuclear coupling. The proton noise-decoupling during the aquisition peroid causes complete spectra. Then a 180° pulse is applied on ^{13}C at the midpoint of the t_1 period, as shown in the timing diagram of Figure 34. This pulse has the effect of exchanging the ^{13}C spin a fixed delay Δ_1 then follows, whose duration is chosen such that the proton doublet components carry out a 180° relative phase shift. Proton nooise-decouping and acquisition start stimultaneously Δ_2 later.

In summary, the 180° carbon pulse has the effect of decoupling in the F_1 dimension, whereas proton noise decoupling provides decoupling in the F_2 dimension. The contour plot of the $^{13}C/^1H$ correlation experiment immediately gives all the proton chemical shifts and their assignments on the basis of their C-H connectivities. Figure 36 clearly illustrates the usefulness of this
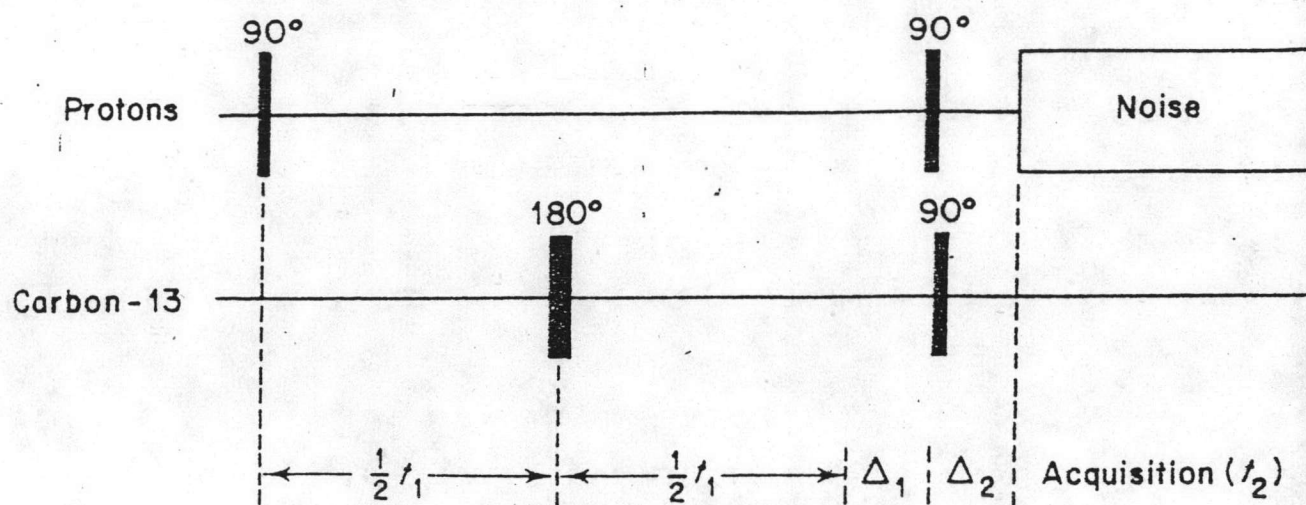
Figure 34   Pulse timing diagram for the $^{13}C-^1H$ chemical shift experiment.
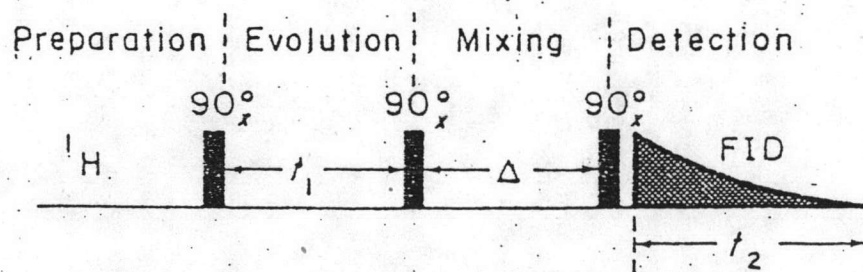

Figure 35   The NOESY pulse sequence.

technique when applied to the complex proton spectrum of methylcyclohexane (32).

3.4 Nuclear Overhauser Enhancement Spectroscopy (NOESY) (32,41)

The important technique in the analysis of the NMR spectra of large molecules is the NOESY experiment. This experiment is on the NOE basis. The NOESY pulse sequence is presented in Figure 35 and consists of three 90° pulse. The first two pulses have the effect as in the COSY experiment. The importance in the NOESY experiment is the time delay (mixing-time) which follows the second pulse. The nuclear overhauser effects require a certain amount of time to build up. The lenght of time chosen for this mixing period depends on the properties of the molecules being investigated. The NOE observed in small molecules, the nuclei have long T_1 and hence long delays are required during which the NOE is built up. In large molecules, T_1 is also reduced hence the NOE builds up in a much shorter time. A 2D spectrum is interpreted in the same way as a COSY spectrum, off diagonal peaks indicating nuclei which are close in space. An example of a NOESY spectrum is presented in Figure 37 (34,44).
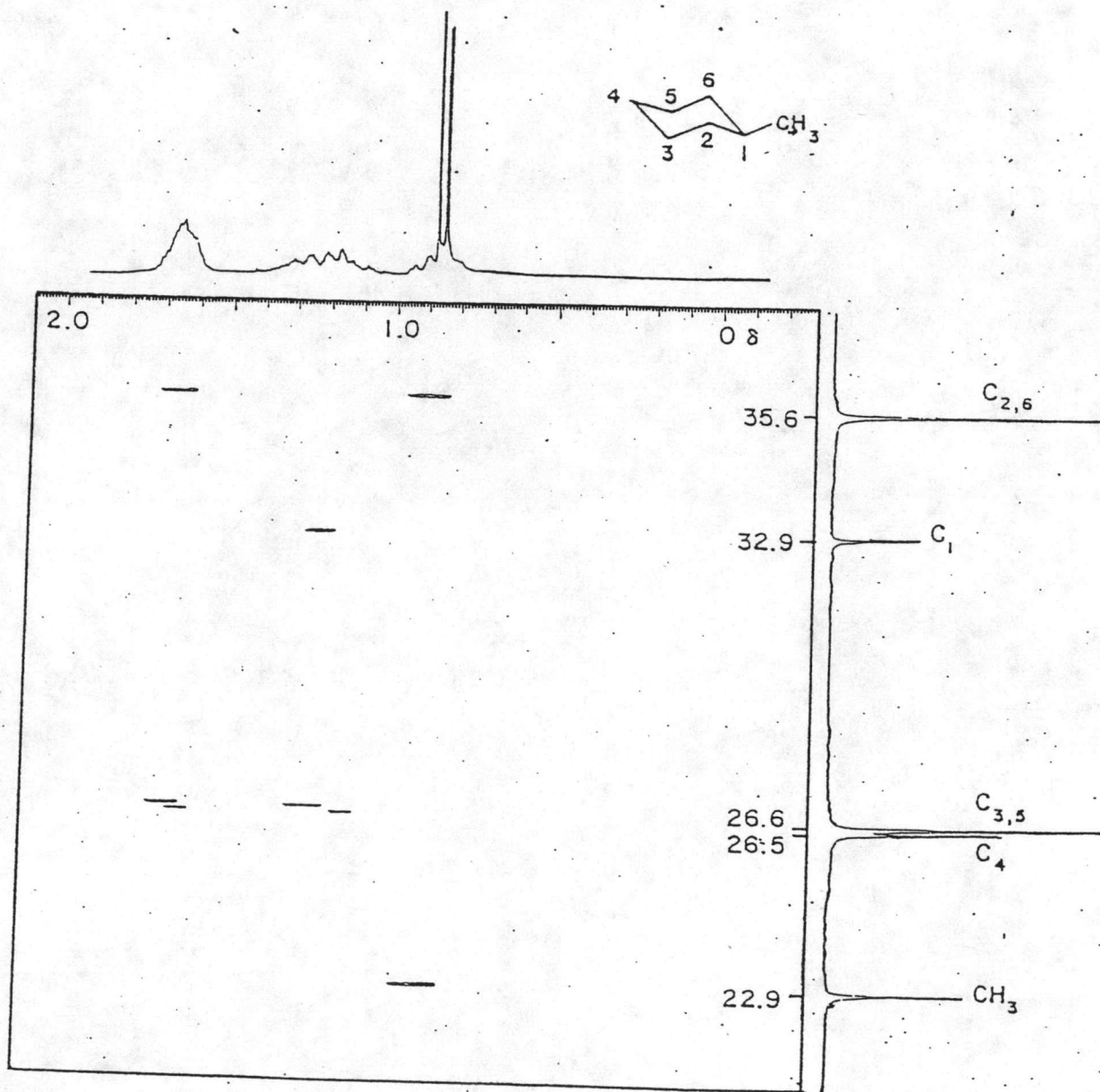
Figure 36   The 2D $^{13}C-^{1}H$ chemical shift correlation plot of Methylcyclohexane with the ^{1}H spectrum along F_1 and the ^{13}C proton noise decoupled spectrum along F_2.
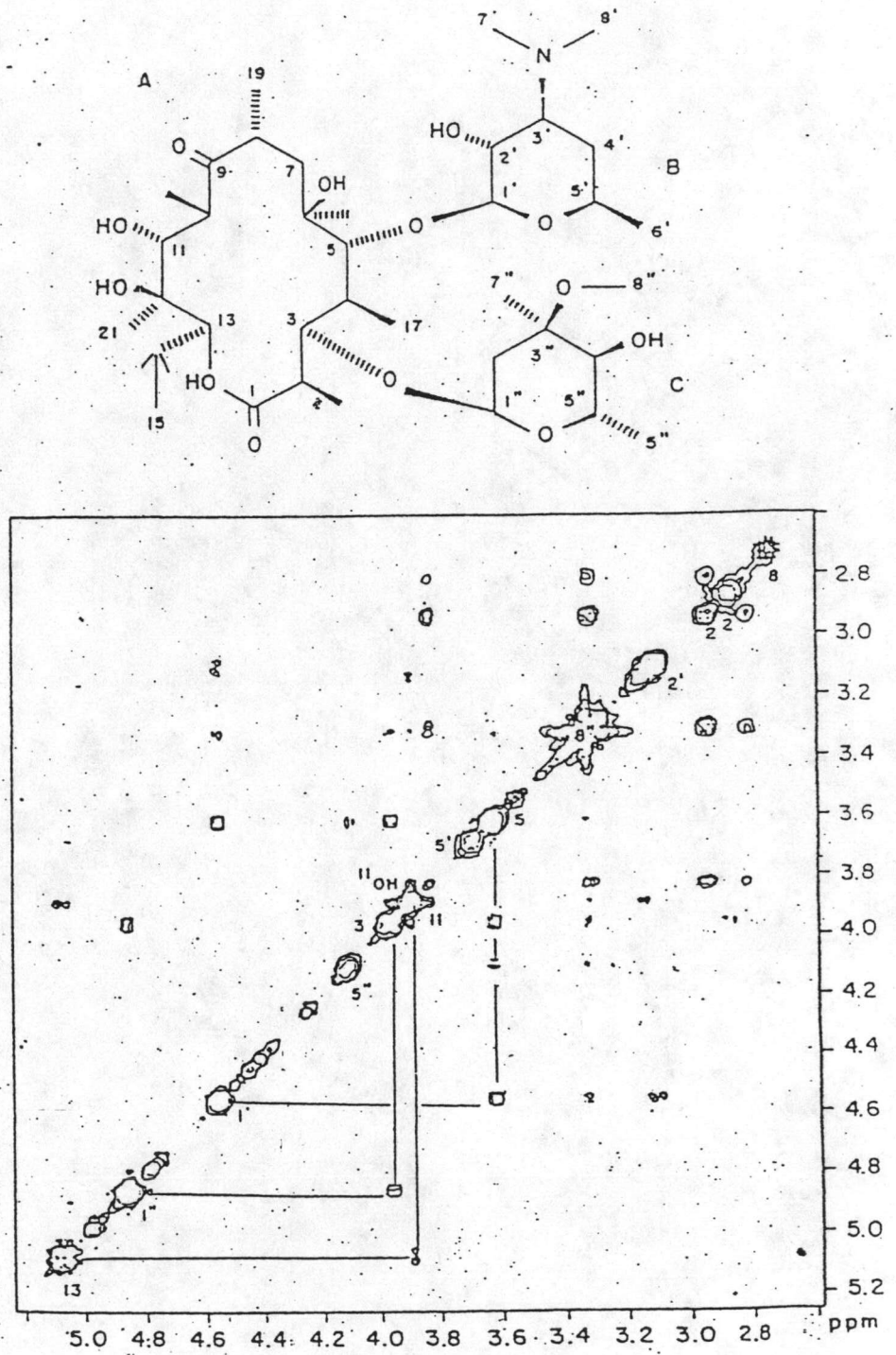
Figure 37   The ^{1}H NMR NOESY spectrum of Erythromycin A